Neurobiology of Disease

Tis21 Knock-Out Enhances the Frequency of Medulloblastoma in Patched1 Heterozygous Mice by Inhibiting the *Cxcl3*-Dependent Migration of Cerebellar Neurons

Stefano Farioli-Vecchioli,[1]* Irene Cinà,[1]* Manuela Ceccarelli,[1]* Laura Micheli,[1]* Luca Leonardi,[1] Maria Teresa Ciotti,[1] Marco De Bardi,[2] Concezio Di Rocco,[3] Roberto Pallini,[3] Sebastiano Cavallaro,[4] and Felice Tirone[1]

[1]Institute of Cell Biology and Neurobiology, National Research Council, Fondazione Santa Lucia, and [2]Neuroimmunology and Flow Cytometry Unit, Fondazione Santa Lucia, 00143 Rome, Italy, [3]Institute of Neurosurgery, Catholic University School of Medicine, 00168 Rome, Italy, and [4]Functional Genomics Center, Institute of Neurological Sciences, National Research Council, 95125 Catania, Italy

A failure in the control of proliferation of cerebellar granule neuron precursor cells (GCPs), located in the external granular layer (EGL) of the cerebellum, gives rise to medulloblastoma. To investigate the process of neoplastic transformation of GCPs, we generated a new medulloblastoma model by crossing *Patched1* heterozygous mice, which develop medulloblastomas with low frequency, with mice lacking the *Tis21* gene. Overexpression of *Tis21* is known to inhibit proliferation and trigger differentiation of GCPs; its expression decreases in human medulloblastomas. Double-knock-out mice show a striking increase in the frequency of medulloblastomas and hyperplastic EGL lesions, formed by preneoplastic GCPs. *Tis21* deletion does not affect the proliferation of GCPs but inhibits their differentiation and, chiefly, their intrinsic ability to migrate outside the EGL. This defect of migration may represent an important step in medulloblastoma formation, as GCPs, remaining longer in the EGL proliferative niche, may become more prone to transformation. By genome-wide analysis, we identified the chemokine *Cxcl3* as a target of *Tis21*. *Cxcl3* is downregulated in *Tis21*-null GCPs of EGL and lesions; addition of Cxcl3 to cerebellar slices rescues the defective migration of *Tis21*-null GCPs and, remarkably, reduces the area of hyperplastic lesions. As *Tis21* activates *Cxcl3* transcription, our results suggest that *Tis21* induces migration of GCPs through *Cxcl3*, which may represent a novel target for medulloblastoma therapy.

Introduction

Cerebellar granule neuron precursor cells (GCPs) intensely proliferate postnatally within the external granular layer (EGL), at the surface of the developing cerebellum (Hatten, 1999). Proliferation of GCPs is triggered by Sonic Hedgehog (Shh), secreted by Purkinje neurons (Dahmane and Ruiz i Altaba, 1999; Wallace, 1999; Wechsler-Reya and Scott, 1999).

The prolonged mitotic activity of GCPs makes them potential targets of transforming insults (Wang and Zoghbi, 2001). In fact, ~25% of medulloblastomas, the tumor of cerebellum and among the most common brain tumors in childhood, arises from GCPs (Kadin et al., 1970; Marino, 2005; Schüller et al., 2008; Yang et al., 2008; Gibson et al., 2010). Other medulloblastoma subtypes may originate from neural precursors of the cerebellar embryonic anlage, different from GCPs and dependent on *Wnt* signaling (Gibson et al., 2010; Hatten and Roussel, 2011).

Inherited or sporadic mutations in the human *Patched1* gene—which encodes the Shh receptor and functions as an inhibitor of the *Shh* pathway in the absence of the ligand—or the lack of one *Patched1* allele in mice models, lead to the development of medulloblastomas, indicating that overactivation of the *Shh* pathway is important in the etiology of the tumor (Hahn et al., 1996, 1998; Goodrich et al., 1997; Pietsch et al., 1997; Raffel et al., 1997; Wolter et al., 1997; Pomeroy et al., 2002; Lee et al., 2003). The Shh-driven proliferation of GCPs in the EGL is maximal 1 week after birth, but after 3 weeks GCPs have differentiated and migrated from the EGL inwardly to the molecular layer (ML) and internal granular layer (IGL), their final destination (Hatten, 1999). In contrast, at the same age, the EGL of *Patched1* heterozygous mice presents clusters of highly proliferating GCPs. These anomalous GCPs, which differ from normal GCPs for their expression profile and for the additional loss of the wild-type Patched1 allele, can be considered a preneoplastic intermediate

Received Jan. 28, 2012; revised Aug. 10, 2012; accepted Sept. 4, 2012.

Author contributions: S.F.-V. and F.T. designed research; S.F.-V., I.C., M.C., L.M., L.L., M.T.C., M.D.B., and S.C. performed research; C.D.R. and R.P. contributed unpublished reagents/analytic tools; S.F.-V., I.C., M.C., L.M., S.C., and F.T. analyzed data; F.T. wrote the paper.

This work was supported by Associazione Italiana Ricerca sul Cancro Grant 9251 (F.T.) and the Italian Ministry of Economy and Finance to Consiglio Nazionale delle Ricerche (Project FaReBio). L.M. was supported by Finanziaria Laziale di Sviluppo. We thank Jane Johnson for the gift of *Math1*-GFP mice and Richard Butler and Maurizia Caruso for critical reading.

This article is freely available online through the *J Neurosci* Open Choice option.

The authors declare no competing financial interests.

*S.F.-V., I.C., M.C., and L.M. contributed equally to this work.

Correspondence should be addressed to Felice Tirone, Institute of Cell Biology and Neurobiology, Consiglio Nazionale Ricerche, Via Fosso di Fiorano 64, 00143 Rome, Italy. E-mail: tirone@inmm.cnr.it.

DOI:10.1523/JNEUROSCI.0412-12.2012

 0270-6474/12/3215547-18$15.00/0

between GCPs and medulloblastoma cells [preneoplastic GCPs (pGCPs)] (Goodrich et al., 1997; Kim et al., 2003; Oliver et al., 2005). Within 3–6 months, in 15–25% of *Patched1* heterozygous mice, the pGCPs will develop into larger lesions and then into tumors (Goodrich et al., 1997; Kim et al., 2003; Kessler et al., 2009).

Tis21, also known as *PC3* or *BTG2* (in mouse, rat, and human, respectively), is a transcriptional cofactor that acts in cerebellar GCPs and in neural progenitor cells of different areas of the brain—such as the hippocampus and the subventricular zone—by inducing them to exit the proliferative state and differentiate (Canzoniere et al., 2004; Farioli-Vecchioli et al., 2008, 2009). *Tis21* inhibits the cell cycle in neural progenitor cells through direct repression of the *cyclin D1* promoter and activates proneural genes through direct repression of the promoter of Id3, an inhibitor of proneural bHLH genes (Canzoniere et al., 2004; Farioli-Vecchioli et al., 2009). Moreover, upregulation of *PC3* (the rat homolog of *Tis21*) in pGCPs within the EGL of *Patched1* heterozygous mice inhibits their proliferation and triggers their differentiation, highly reducing the incidence of medulloblastoma (Farioli-Vecchioli et al., 2007).

Considering that *Tis21* is downregulated in human medulloblastomas (Farioli-Vecchioli et al., 2007), we asked whether the transformation of pGCPs is affected by a loss of the *PC3*-dependent control of proliferation and differentiation.

We found that genetic ablation of *Tis21* greatly induced the frequency of medulloblastoma in Patched1 heterozygous mice without affecting the proliferation of GCPs, but reducing their differentiation. Chiefly, however, ablation of *Tis21* impaired the process of migration from the EGL and lesions to the IGL. This migration defect appears to be dependent on Cxcl3, as it is rescued by this chemokine, and may play a critical effect on the conversion of pGCPs into tumor cells.

Materials and Methods

Mouse lines and genotyping. The *Tis21* knock-out mice have been generated previously as described previously (Park et al., 2004) in C57BL/6 (B6) strain by replacing with the neomycin resistance cassette exon II of the Tis21 gene. *Patched1* heterozygous mice (*Ptch1*$^{+/-}$) were generated in a CD1 background through disruption of exons 6 and 7 (Hahn et al., 1998). *Ptch1*$^{-/-}$ embryos die before E14. The crossing of *Patched1* heterozygous with *Tis21*$^{-/-}$ mice generated *Patched1/Tis21* double-mutant mice that were interbred to obtain the genotypes studied; the progeny was made isogenic before starting any analysis, by further interbreeding for six or more generations.

Math1-green fluorescent protein mice (*Math1*-GFP) express GFP driven by the Math1 enhancer (Lumpkin et al., 2003). Genotyping of *Patched1*/*Tis21* mice was routinely performed by PCR, using genomic DNA from tail tips. To identify mice carrying the *Tis21* null or wild-type alleles, three pairs of primers were used, one complementary to the neo cassette and the others complementary either to exon I or to the targeted exon II, and were amplified together in the PCR to obtain different patterns of amplification specific for each allele: neo(−), 5′-GATGCCTGCTTGCCGAATAT-3′; exI(+), 5′-TCTCCAGTCCTCCTGAGGACT-3′; exII(−), 5′-GCCATCACATAGTTCTTCGAG-3′. *Patched1* wild-type and *Patched1*-null alleles were identified by PCR using three pairs of primers complementary to the neo insert and wild-type regions of Patched1 knock-out mice, as described previously (Hahn et al., 1998; Farioli-Vecchioli et al., 2007). *Math1*-GFP mice were crossed with Patched1/Tis21 double knock-out mice to obtain *Ptch1*$^{+/-}$/*Tis21*$^{+/-}$/*Math1*-GFP$^{+/-}$ mice, which were interbred at least four times before further analysis, in this way generating the different genotypes under study. Genotyping of *Math1*-GFP pups was performed using a "GFP flashlight" (Nightsea) that made the GFP^{+} pups glow.

Experiments were performed with mice of either sex, and all animal procedures were completed in accordance with the current European (directive 2010/63/EU) Ethical Committee guidelines.

Tumor and lesion quantification and histological analysis. Mice were observed for symptoms of medulloblastoma daily for a period of 12 months. On the appearance of symptoms of medulloblastoma (head doming, hunched posture, preferential turning to one side, severe weight loss, paralysis, ruffling of fur, or inactivity), they were killed and autopsied. The cerebellar tumor was either snap frozen in liquid nitrogen for mRNA studies, or fixed in 4% paraformaldehyde (PFA) by immersion overnight, and then cryoprotected before sectioning in 30% sucrose in PBS–DEPC. Samples were then embedded in Tissue-Tek OCT (Sakura Finetek), sectioned serially, and stained with hematoxylin/eosin to confirm by histological analysis that the necropsied brain tissue was medulloblastoma. Lesions were identified by visualizing the GFP^{+} proliferating GCPs in asymptomatic *Ptch1*$^{+/-}$/*Tis21*$^{-/-}$/*Math1*-GFP^{+} mice.

Bromodeoxyuridine treatment of mice. GCPs entering in S-phase were visualized 1 h after an injection of bromodeoxyuridine (BrdU) (95 mg/kg, i.p.), according to existing protocols (Canzoniere et al., 2004; Qiu et al., 2010).

Immunohistochemistry: sample preparation, BrdU labeling, antibodies, and image analysis. Histology and immunostaining of sections, stained for multiple labeling and BrdU incorporation using fluorescent methods, was performed as described previously (Canzoniere et al., 2004; Farioli-Vecchioli et al., 2007). Briefly, cerebella of P7 (i.e., 7 d of age) and P14 mice (for EGL or lesion analysis) were dissected out and fixed by immersion overnight in 4% PFA in PBS–DEPC, whereas cerebella of P42 and P84 mice (for lesion analysis) were dissected out after transcardiac perfusion with 4% PFA in PBS–DEPC and kept overnight in PFA. Fixed cerebella were cryoprotected before sectioning in 30% sucrose in PBS–DEPC overnight at 4°C and frozen at −80°C until use. Cerebella were then embedded in Tissue-Tek OCT (Sakura Finetek), and midsagittal sections of 20 μm were cut on a rotary microtome. Lesion studies (proliferation, differentiation, apoptosis, migration, and volume quantifications) were performed on free-floating sagittal sections 40 μm thick. BrdU incorporation was detected following pretreatment of sections to denature the DNA, with 2N HCl 45 min at 37°C and then with 0.1 M sodium borate buffer, pH 8.5, for 10 min. Primary antibodies used were a rat monoclonal antibody against BrdU (AbD Serotec; MCA2060; 1:150), a mouse monoclonal antibody raised against NeuN (Millipore Bioscience Research Reagents; MAB377; 1:100), a goat polyclonal antibody against NeuroD1 (R&D Systems; AF2746; 1:100), or rabbit polyclonal antibodies against cleaved (activated) Caspase-3 (Cell Signaling Technology; 9661; 1:100) or Cxcr2 receptor (Santa Cruz Biotechnology; sc-682; 1:200). Secondary antibodies used to visualize the antigen were either donkey anti-rat IgG tetramethylrhodamine isothiocyanate (TRITC)-conjugated (Jackson ImmunoResearch; BrdU), or donkey anti-rabbit TRITC-conjugated (Jackson ImmunoResearch; Caspase-3), donkey anti-goat Cy2-conjugated (Jackson ImmunoResearch; NeuroD1), or donkey anti-mouse Cy2-conjugated and Alexa 647-conjugated (Invitrogen; NeuN).

Images of the immunostained sections were obtained by laser-scanning confocal microscopy using a TCS SP5 microscope (Leica Microsystems) and were analyzed by the I.A.S. software (Delta Sistemi).

Quantification of cell numbers in EGL and lesions. Quantifications of proliferating, differentiating, or apoptotic cells in the EGL were performed on five nonadjacent midsagittal sections at the midpoint of the fifth, seventh, and ninth folia of each section, analyzing five sections per mouse and three mice for each genotype. The EGL cell number was expressed as percentage ratio of proliferating (BrdU^{+}), differentiating (NeuroD1^{+} or NeuN^{+}), or apoptotic (cleaved Caspase-3^{+}) cells, to the total number of cells (labeled by Hoechst 33258; 1 mg/ml in PBS), counted for the entire length of the EGL in each photomicrograph field, from digital images.

BrdU^{+}, NeuroD1^{+}, NeuN^{+}, or cleaved Caspase-3^{+} cells in lesions were counted in the whole lesion area, defined by the presence of GFP^{+} cells, on at least five nonadjacent midsagittal sections per lesion. We

examined all lesions present in each mouse analyzed, whose number for each genotype and time point is indicated in Figure 2*E*.

Cell migration assays, layer areas, lesion areas, and volumes. In experiments of migration from the EGL, the number of BrdU-labeled cells in each defined layer (i.e., EGL, ML, or IGL) was counted as percentage of total BrdU-labeled cells in all three layers, in five nonadjacent midsagittal sections at the midpoint of the fifth, seventh, and ninth folia. Three mice per genotype were analyzed. Similarly, in experiments of migration from lesions, the number of BrdU-labeled cells was counted in each defined layer neighboring the lesion (i.e., ML and IGL) as percentage of total BrdU-labeled cells present in the lesion and layers, in three nonadjacent sagittal sections per lesion.

Planimetric measurements of the EGL, ML, or IGL and lesion area were performed for the whole length of the layer or for the whole extension of the lesion in each (5×) photomicrograph field. The area was obtained by tracing the outline of the whole layer or lesion on a digital picture captured and measured using the I.A.S. software (Delta Sistemi).

The volume of each lesion was calculated multiplying the average lesion area by section thickness and by number of sections in which the lesion was observed.

Isolation of cerebellar granule progenitor cells (from EGL and lesions). GCPs were isolated from cerebella of P7 mice or of P7 Wistar rats following a described procedure, consisting in the enzymatic digestion of cerebella chopped into small pieces, followed by separation onto a step gradient of 35 and 65% Percoll and then by depletion of adherent cells with two consecutive incubations on tissue culture dishes (Wechsler-Reya and Scott, 1999).

Organotypic slice cultures (BrdU labeling, retroviral infection, and immunostaining). Slices were taken and cultured following the methods of Stoppini et al. (1991) and Polleux et al. (1998). Briefly, the brains of P7 pups from the different genotypes were isolated under aseptic condition following decapitation, the meninges were removed, and the cerebellum was isolated from the rest of the brain. Cerebella were cut on a McIlwain tissue chopper into 350-μm-thick parasagittal slices. After cutting, slices were washed in calcium- and magnesium-free HBSS with 36 mM glucose and 15 mM HEPES, pH 7.4, for 30 min at 4°C, carefully separated, and transferred to 23-mm-diameter semiporous membrane culture inserts with a 0.4 μm pore size (Falcon cell culture inserts; BD Biosciences Discovery Labware) with culture medium containing DMEM/Ham's F-12 with N2 supplement (Invitrogen), 20 mM KCl, 36 mM glucose, and penicillin–streptomycin.

For migration experiments, slices were cultured for 120 h with 100 ng/ml Cxcl3 (R&D Systems) or with vehicle (PBS, 0.1% BSA) alone, and the medium was replaced every 48 h. To label and subsequently track migrating cells from EGL, cultures were pulse-labeled with BrdU (10 μg/ml; Sigma-Aldrich) added at t0 for 18 h. In experiments of retroviral infection with the cDNA sequence of *Tis21*, organotypic slices were infected by adding directly onto the slice the volume of viral stock (pCAG-Tomato-*Tis21* retrovirus) corresponding to 1.4×10^6 TU (Boukhtouche et al., 2006), pulsed the day after with 10 μg/ml BrdU for 6 h, and cultured for an additional 72 h. For each animal, one-half of the cerebellar slices served as control and were infected with pCAG-Tomato-empty virus and the other one-half with pCAG-Tomato-*Tis21*. At the end of each experiment, slices were fixed in 4% PFA and immunostained. For proliferation and differentiation experiments, slices were cultured for 48 h with 100 ng/ml Cxcl3 (R&D Systems) or with vehicle alone (PBS, 0.1% BSA); after a 2 h pulse with BrdU, slices were fixed and analyzed for incorporation of BrdU and expression of NeuroD1 or NeuN. For retroviral experiments, a goat polyclonal DsRed antibody (Santa Cruz) was used at 1:100 in 5% normal donkey serum overnight at 4°C.

In vitro *migration assay.* The migration of GFP^+ GCPs purified from GFP P7 mice was measured using poly-D-lysine-coated membranes (0.1 mg/ml; Sigma-Aldrich) with 8 μm pore size (0.3 cm^2) in modified Boyden chambers as previously described (Lu et al., 2001). To obtain GCPs, cerebella were removed, chopped into small pieces, and resuspended in HBSS Ca–Mg-free with 0.5 mM EDTA through Pasteur pipettes of two sequentially decreasing bore size (10 times each). The cell resuspension was then passed through a 30 μm cell strainer (BD Biosciences). The filtrate was centrifuged at 200 × *g* to sediment the dissociated cells, resuspended in 200 μl of PBS with 5 mM EDTA, and separated by fluorescence-activated cell sorting (FACS) on a MoFlo high-speed cell sorter (Beckman Coulter). Isolated GCPs were resuspended in 200 μl of DMEM/Ham's F-12 with 1% fetal bovine serum and directly seeded (1×10^5) onto the membrane filter in the upper chamber (BD Biosciences; 353182). In the lower chamber, medium with 5% fetal bovine serum was added in order to establish a 1–5% serum gradient. After 16 h at 37°C in 5% CO_2, cells were removed from the upper membrane using cotton swab and washing twice with PBS. The cells on the lower surface were fixed in 4% PFA, stained with Hoechst 33258, and counted by confocal microscopy. Twenty randomly chosen high-magnification fields were counted in each well; three experiments were performed.

Design of small interference RNAs and transfection of GCPs. Several 19 nt small interference RNAs (siRNAs) specific to Cxcl3 were designed by the on-line Design Tool software (MWG); two of them (siRNA7-*Cxcl3* and siRNA6-*Cxcl3*, the latter specific to both mouse and rat sequences) were selected for their ability to inhibit Cxcl3 expression. GCPs were transfected immediately after the preparation of the cell suspension from P7 rat cerebella, according to a described protocol (Zhokhov et al., 2008). For this procedure, we used an electroporation-based Amaxa Nucleofector technology (rat neuron nucleofection kit; Amaxa Biosystems). The siRNA7-Cxcl3 sequence was 5′-ACAAGGTCGTCTCAGTGTA-3′; the siRNA6-Cxcl3 sequence was 5′-CAACTCCTGAGA GTTCATA-3′; the control siRNA was from the luciferase gene, 5′-CTTACGCTGAGT ACTTCGA-3′. For each transfection procedure, 6×10^6 GCPs were centrifuged for 2 min at 100 × *g* and then resuspended in 100 μl of transfection buffer; 15 μg of either siRNA7-*Cxcl3* or siRNA6-*Cxcl3*, or of siRNA-control, previously dissolved in the same buffer, was then added. Transfection was performed in cuvettes part of the kit. Transfected GCPs were suspended in DMEM with 10% fetal bovine serum and plated in uncoated 35 mm dishes for 3 h under gentle agitation, then resuspended in DMEM/Ham's F-12 with 1% fetal bovine serum and seeded onto the membrane filter of the modified Boyden chamber for migration analysis for 16 h, as described above (see *In vitro* migration assay). Alternatively, transfected GCPs were plated in coated dishes for 4 h, and then the medium was replaced with serum-free DMEM/Ham's F-12 with N2 supplement, and after 16 h, GCPs were analyzed for differentiation or collected for RNA analysis.

Transfection of cerebellar slices. Cerebellar slices were isolated from P7 mice and incubated for 4 h onto semiporous membrane, as described previously [see above, Organotypic slice cultures (BrdU labeling, retroviral infection, and immunostaining)]. siRNA targeting *Cxcl3* (siRNA6-*Cxcl3*) or siRNA-control was incubated for 20 min with 8 μl of Lipofectamine 2000. The medium of cerebellar slices was then substituted with the transfection mixture added to serum-free N2 medium with 20 nM final concentration of each siRNA (1.5 ml total volume, 1 ml at bottom of cultures, 0.5 ml at top of slices). After 16 h, the siRNA-containing medium was replaced with regular serum-free N2-supplemented medium containing BrdU, replaced again after 6 h with medium without BrdU, and left for 72 h. Then the percentage of GCPs migrated out of EGL (BrdU+) was determined.

DNA constructs and retrovirus production. The retroviral vector pCAG-IRES-tdTomato, kindly provided by Dr. Mu-ming Poo (University of California, Berkeley, Berkeley, CA) (Cancedda et al., 2007), was used to express the cDNA of *Tis21* (i.e., the murine sequence) only in dividing GCPs. The full open reading frame of *Tis21* cDNA was cloned in the sites XhoI-5′/SmaI-3′ of pCAG-IRES-tdTomato, obtaining pCAG-IRES-tdTomato-*Tis21*. The construct was checked by DNA sequencing.

Retroviruses were propagated as previously described (Farioli-Vecchioli et al., 2008).

RNA extraction, real-time RT-PCR. Total RNA, extracted from GCPs and reverse-transcribed as described previously (Guardavaccaro et al., 2000), was analyzed by real-time RT-PCR amplification, using TaqMan probe-based fluorogenic 5-nuclease chemistry in duplicate samples and a 7900HT System (Applied Biosystems). The mRNA relative expression values, obtained by the comparative cycle threshold method (Livak and Schmittgen, 2001), were normalized to endogenous controls TATA-binding protein and GAPDH. Statistical analysis of mRNA expression values was performed by Student's *t* test on data normalized to the en-

dogenous controls but not relativized in fold expression of the calibrator sample. Specific real-time RT-PCR primers were designed by the software Beacon Designer 7.1 (Premier Biosoft International); their sequence is available on request.

Microarray analysis. Genome-wide expression analysis of GCPs isolated from the EGL of P7 mice was performed with Whole Mouse Genome Microarrays (Agilent Technologies). Significant changes in gene expression were identified when comparing *Tis21*-null and *Tis21* wild-type mice, either in *Patched1* wild-type background ($Ptch1^{+/+}/Tis21^{-/-}$ vs $Ptch1^{+/+}/Tis21^{+/+}$) or in *Patched1* heterozygous background ($Ptch1^{+/-}/Tis21^{-/-}$ vs $Ptch1^{+/-}/Tis21^{+/+}$). Following extraction of GPCs from $Ptch1^{+/+}/Tis21^{+/+}$ ($n = 3$), $Ptch1^{+/+}/Tis21^{-/-}$ ($n = 3$), $Ptch1^{+/-}/Tis21^{+/+}$ ($n = 4$), and $Ptch1^{+/-}/Tis21^{-/-}$ ($n = 4$) mice with Trizol (Invitrogen), RNA integrity was confirmed by using a RNA chip and a 2100 Bioanalyzer (Agilent Technologies) with the protocol outlined by the manufacturer. cRNAs labeled with Cy3-CTP were synthesized from 1 μg of total RNA of each sample using the Low Input Quick Amp Labeling Kit (Agilent Technologies) following the manufacturer's protocol. A reference cRNA, labeled with Cy5-CTP was synthesized from 1 μg of RNA from adult mouse brain. Aliquots (750 ng) of Cy3- and Cy5-labeled cRNA targets were cohybridized on Whole Mouse Genome Microarrays (Design ID 014868; Agilent Technologies). Microarray hybridization and washing were performed using reagents and instruments (hybridization chambers and rotating oven) as indicated by the manufacturer (Agilent Technologies). Microarrays were scanned at 5 μm resolution using a GenePix Personal 4100A microarray scanner and the GenePix Pro 6.0 acquisition and data extraction software (Molecular Devices). Raw data were processed and analyzed by GeneSpring 11.5.1 (Agilent Technologies). Raw signal values were thresholded to 1, $\log_2$ transformed, normalized to the 50th percentile, and baselined to the median of all samples. Genes with a corrected p value of <0.05 (one-way ANOVA followed by the Benjamini and Hochberg false discovery rate and the Tukey's *post hoc* test) were considered differentially expressed.

Chromatin immunoprecipitation. Primary cultures of cerebellar postmitotic granule neurons from Wistar P7 rats were prepared and infected with adenoviruses expressing *Tis21* (rat sequence) or β-galactosidase (β-Gal) as previously described (Canzoniere et al., 2004; Farioli-Vecchioli et al., 2007). Chromatin was released from nuclear preparations of cerebellar granule neurons infected with adeno-*Tis21* or adeno-β-*Gal* by digestion at 37°C with micrococcal nuclease (to obtain fragments of predominantly one to five nucleosomes) and immunoprecipitated with anti-Tis21 antibody as previously described (O'Neill and Turner, 1995; Farioli-Vecchioli et al., 2009). Approximately 4×10^7 cerebellar granule neurons were used for each immunoprecipitation, either with anti-Tis21 A3H antibody or with normal rabbit serum as control. Alternatively, an equivalent number of rat GCPs were used for chromatin immunoprecipitation (ChIP) assays, isolated as described above. The immunoprecipitated DNA and 1/200 dilution of the input DNA were quantified in triplicate samples by real-time PCR using the 2^{-Ct} formula. The DNA immunoprecipitated by immune serum and by normal rabbit serum was calculated as input percentage for each cell treatment. Input percentage is the ratio of the average value of the DNA detected in immunoprecipitated samples to the average value of the DNA present in input lysates (Heard et al., 2001). The amount of DNA promoter immunoprecipitated was finally expressed as fold enrichment (ratio of input percentage of DNA immunoprecipitated by A3H antibody to input percentage of DNA immunoprecipitated by normal rabbit serum). PCR primers used to amplify were as follows: (1) Cxcl3 promoter region 170 nt before transcription start, 5′-TTCTTCTGACACAGGGAC-3′, 5′-ATACATGATGGCTG GAAGA-3′; (2) muscle creatine kinase promoter region 340 nt before transcription start, 5′-GGCTGAGGGCAGGCTGTAAC-3′, 5′-GGGTCAGTAATACTCTGGGTGTCC-3′.

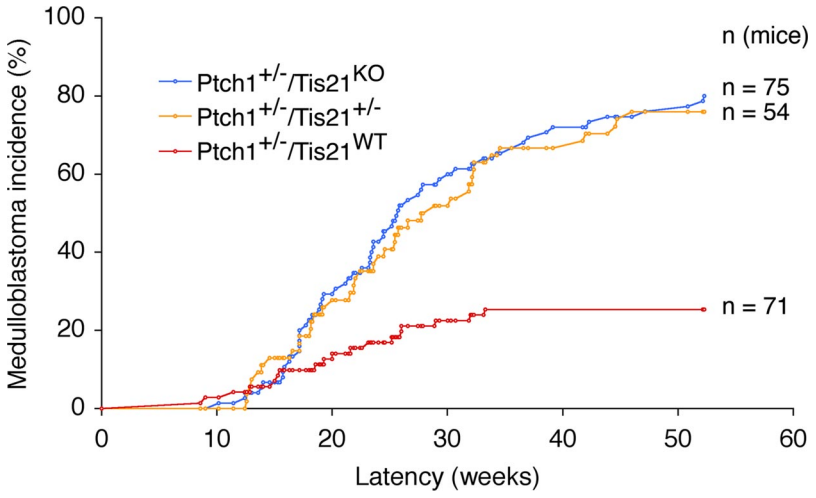

Figure 1. Enhancement of medulloblastoma incidence in *Patched1* heterozygous mice deprived of *Tis21*. $Ptch1^{+/-}/Tis21^{WT}$, $Ptch1^{+/-}/Tis21^{+/-}$ and $Ptch1^{+/-}/Tis21^{KO}$ mice, obtained by interbreeding for at least six generations the progeny of *Patched1* heterozygous and *Tis21* knock-out mice, were then monitored for the onset of medulloblastoma; $p < 0.0001$ vs $Ptch1^{+/-}/Tis21^{WT}$, χ^2 test (Table 1).

In situ *hybridization.* Preparation of sections and hybridization were performed as previously described (Canzoniere et al., 2004). Antisense riboprobes detecting mouse *Cxcl3* and *Tis21* mRNAs were synthesized by T7 polymerase from the 3′-UTR region of mouse *Cxcl3* and *Tis21* cDNAs (a 300-bp-long sequence part of the fourth exon of the Cxcl3 gene and a 350-bp-long sequence within the second exon of the *Tis21* gene, chosen for the absence of any cross-homology). The *Cxcl3* and *Tis21* cDNA probes had been previously cloned into the pcDNA3 vector in the NotI site and were checked by sequencing. Riboprobes were labeled with digoxigenin-UTP (transcription kit; Roche), according to the protocol of the manufacturer. No signal was detected by sense probes.

Cxcl3 promoter activity. Postmitotic cerebellar granule neurons, or the tet-off PC12 cell line expressing a doxycycline-regulated *Tis21* cDNA (rat sequence) (Farioli-Vecchioli et al., 2009), were seeded in 35 mm poly-lysine-coated dishes (2×10^6 or 5×10^5 cells per dish, respectively). The following day, cerebellar granule neurons were transfected with a vector expressing *Tis21* (rat sequence, pSCT-*Tis21*) (Guardavaccaro et al., 2000) and with the pGL3-Cxcl3-prom/-628 reporter construct using the Lipofectamine reagent and were harvested after 48 h. PC12 cells were transfected only with the pGL3-Cxcl3-prom/-628 reporter, and *Tis21* expression was activated by removing doxycycline from the medium. Luciferase assays were performed by the Dual-Luciferase reporter assay system (Promega) according to the manufacturer's instructions and as previously described (Canzoniere et al., 2004). Luciferase activities were measured in luciferase units per microgram of protein normalized to the activity of the coreporter pRL-TK present in each extract, as a measure of the efficiency of transfection. The pGL3-*Cxcl3*-prom/-628 construct had been generated by cloning the PCR-amplified region of the rat *Cxcl3* promoter (628 nt before transcription start), using genomic rat DNA as template, in the 5′-SacI-3′-BglII site of pGL3-basic. The construct was checked by sequencing.

Results

Tis21 ablation facilitates tumorigenesis

Patched1 heterozygous mice ($Ptch1^{+/-}$), with low frequency, develop spontaneous medulloblastoma from pGCPs clustering in the EGL (Kessler et al., 2009). To test whether the tumorigenicity of pGCPs is affected by ablation of *Tis21*, we analyzed the frequency of medulloblastomas developed during 1 year of life in $Ptch1^{+/-}$ mice crossed with *Tis21* knock-out mice. We observed that, while $Ptch1^{+/-}/Tis21^{WT}$ mice developed medulloblastoma with a frequency of 25.3%, double-mutant mice, either $Ptch1^{+/-}/$

Table 1. Statistical analysis of medulloblastoma incidence and latency[a]

Genotype	$Tis21^{WT}$	$Tis21^{KO}$	$Ptch1^{+/-}/Tis21^{WT}$	$Ptch1^{+/-}/Tis21^{+/-}$	$Ptch1^{+/-}/Tis21^{KO}$
Medulloblastoma (%)	0 (0.0)	0 (0.0)	118 (25.35)	41* (75.93)	60* (80.00)
Average latency (weeks)	—	—	20.09 ± 1.7	25.46 ± 1.5†	25.57 ± 1.3†
No. of mice analyzed	40	42	71	54	75

[a]The five genotypes refer to the progeny of breedings between Patched1 heterozygotes and Tis21 knock-out mice; all mouse genotypes are in the same genetic background, having been cross-mated for at least six generations.

*$p < 0.0001$ versus $Ptch1^{+/-}/Tis21^{WT}$ group (χ^2 test).

†$p < 0.05$ versus $Ptch1^{+/-}/Tis21^{WT}$ group (Student's t test).

$Tis21^{KO}$ or $Ptch1^{+/-}/Tis21^{+/-}$, showed a significantly higher incidence of medulloblastoma [i.e., 80% ($p < 0.0001$) and 75.9% ($p < 0.0001$), respectively] (Fig. 1, Table 1). Unexpectedly, however, the average tumor latency was significantly longer in double-mutant than in $Ptch1^{+/-}/Tis21^{WT}$ mice (Table 1). No tumors developed in $Ptch1^{+/+}/Tis21^{-/-}$ or $Ptch1^{+/+}/Tis21^{+/+}$ mice (hereafter referred to as $Tis21^{KO}$ and $Tis21^{WT}$; Table 1). Therefore, the ablation of one or both alleles of *Tis21* appears to strongly favor tumorigenesis *in* $Ptch1^{+/-}$ pGCPs.

To investigate such a *Tis21*-dependent effect, we analyzed key cellular parameters of the pGCPs resident within the lesions (i.e., proliferation, differentiation, viability, and migration).

Patched1 heterozygous mice at P14 present lesions, characterized by thicker EGL regions, expanded as nodular formations inside the cerebellar lobules and containing highly proliferating pGCPs. These lesions are defined hyperplastic EGL remnants or focal hyperplasias if comprising >30 pGCPs, or diffuse hyperplasias when including >5000 cells (Kim et al., 2003; Thomas et al., 2009). Focal hyperplasias are frequent at P14, but starting from P21 they begin to disappear, being substituted by larger diffuse hyperplasias, which indicates the occurrence of a selection of pGCPs into tumor cells (Kim et al., 2003; Thomas et al., 2009).

Thus, we analyzed the early hyperplasia lesions at P14, when normal GCPs in the EGL are two to three layers thick, having almost completed their migration within the IGL, and the remaining clusters of GCPs can be considered preneoplastic. We also analyzed lesions at 6 and 12 weeks, when the EGL has disappeared and the external cerebellum contains foci of ectopic pGCPs (Oliver et al., 2005).

To identify pGCPs in focal and diffuse hyperplasia lesions, double-mutant $Ptch1^{+/-}/Tis21^{KO}$ mice were crossed with *Math1*-GFP transgenic mice (hereafter referred to as GFP) (Lumpkin et al., 2003), carrying the GFP transgene under control of the enhancer of Math1, a transcription factor expressed in proliferating, normal, preneoplastic, and tumor GCPs (Ben-Arie et al., 2000; Kim et al., 2003; Lee et al., 2003; Oliver et al., 2005). We verified that the progeny of $Ptch1^{+/-}/Tis21^{KO}$ double mutants crossed with GFP mice presented frequency and volumes of lesions and proliferative parameters of pGCPs equivalent to those of double mutants not crossed with GFP mice (data not shown).

We observed that the percentage of $Ptch1^{+/-}/Tis21^{KO}$/GFP mice with focal or diffused hyperplasia lesions ranged between 100 and 80% at 2, 6, and 12 weeks after birth, whereas that of $Ptch1^{+/-}/Tis21^{WT}$/GFP mice was significantly lower at 2 weeks (60%) and decreased to 20% within 12 postnatal weeks (Fig. 2*A*,*B*; $Ptch1^{+/-}/Tis21^{KO}$/GFP vs $Ptch1^{+/-}/Tis21^{WT}$/GFP; $p = 0.02$ and $p = 0.03$ in 2- and 12-week-old mice, respectively). Interestingly, the percentage of mice with lesions at 12 weeks matched exactly in both genotypes the percentage of mice developing medulloblastoma (Fig. 2*B*, Table 1), indicating that lesions present at 12 postnatal weeks are irreversible. Furthermore, we observed that the number of hyperplasia lesions per mice was significantly higher in $Ptch1^{+/-}/Tis21^{KO}$/GFP mice at 2 and 6 weeks of age, although this number progressively decreased, matching, at 12 weeks, that observed in $Ptch1^{+/-}/Tis21^{WT}$/GFP mice (Fig. 2*A*,*C*; $Ptch1^{+/-}/Tis21^{KO}$/GFP vs $Ptch1^{+/-}/Tis21^{WT}$/GFP; $p = 0.006$ and $p = 0.02$ in 2- and 6-week-old mice, respectively). In both genotypes, we observed a progressive increase of lesion volume through successive ages; at 2 weeks of age, however, lesion volumes were significantly greater in double mutants than in Patched1 heterozygous mice (Fig. 2*A*,*D*; $Ptch1^{+/-}/Tis21^{KO}$/GFP vs $Ptch1^{+/-}/Tis21^{WT}$/GFP; $p = 0.007$; the number of mice analyzed in Fig. 2*B–D* is shown in Fig. 2*E*).

As a whole, these results suggested that, in $Ptch1^{+/-}/Tis21^{KO}$ double-mutant mice, pGCPs were more prone to cluster in lesions and expand into tumors, although with a longer latency than in Patched1 heterozygous mice.

We reasoned that the higher incidence of tumors observed in double mutants could depend on the greater frequency and persistence of lesions. To better understand this aspect, we analyzed pGCPs inside lesions, whose area was visualized by the presence of GFP^+ cells. We measured the proliferation rate of pGCPs through BrdU incorporation after a pulse of 1 h, their differentiation, by labeling pGCPs with the neural markers NeuroD1 and NeuN, and their survival. No significant differences were detected between $Ptch1^{+/-}/Tis21^{KO}$/GFP and $Ptch1^{+/-}/Tis21^{WT}$/GFP mice in the number of either $BrdU^+$, $NeuroD1^+$, or $NeuN^+$ cells present within the GFP^+ lesion area, at 2, 6, or 12 weeks of age (data not shown). Conversely, we observed a significant increase of apoptosis at 6 weeks of age in $Ptch1^{+/-}/Tis21^{KO}$/GFP versus $Ptch1^{+/-}/Tis21^{WT}$/GFP mice, as determined by counting the number of cleaved $Caspase\text{-}3^+$ cells per lesion area (Fig. 3*A*,*B*; $p = 0.01$). Then, we measured the percentage of pGCPs migrated outside lesions by labeling proliferating pGCPs in mice of 2 and 6 weeks of age with a pulse of BrdU, and following their migration to the ML and IGL over the next 5 d. An evident reduction (>40%) in the percentage of $BrdU^+$ pGCPs migrated from the lesion to both the ML and IGL was observed in $Ptch1^{+/-}/Tis21^{KO}$/GFP mice at either 2 or 6 weeks of age (Fig. 3*C–E*; $Ptch1^{+/-}/Tis21^{KO}$/GFP vs $Ptch1^{+/-}/Tis21^{WT}$/GFP mice, ML: $p = 0.007$ at 2 weeks, $p = 0.03$ at 6 weeks of age; IGL: $p = 0.007$ at 2 weeks, $p = 0.02$ at 6 weeks of age). As a whole, these data indicate that ablation of *Tis21* impairs the migration of pGCPs outside lesions and suggest that this defect, by delaying the disappearance of lesions from the proliferative area at the surface of cerebellum, favors their conversion into medulloblastoma.

Tis21 ablation inhibits differentiation and migration of GCPs

Having analyzed the pGCPs inside hyperplastic lesions, we sought to define whether the genetic ablation of Tis21, alone ($Tis21^{KO}$ mice) or combined with that of one Patched1 allele ($Ptch1^{+/-}/Tis21^{KO}$ mice), affected the proliferation and differentiation of GCPs in lesion-free areas of the EGL at P7 and P14. These stages precede or correspond to the initial formation of focal hyperplasia lesions, respectively.

At P7—the age of highest expansion of GCPs—the percentage of proliferating GCPs, identified by incorporation of BrdU after

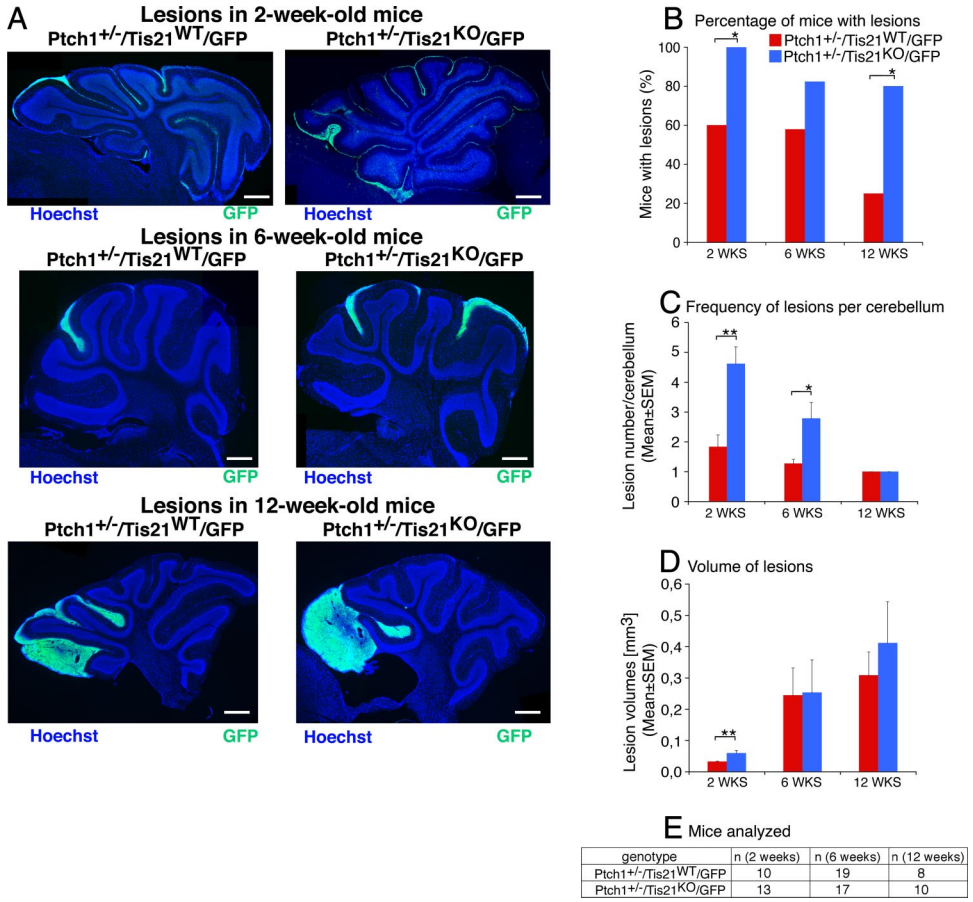

genotype	n (2 weeks)	n (6 weeks)	n (12 weeks)
Ptch1+/-/Tis21WT/GFP	10	19	8
Ptch1+/-/Tis21KO/GFP	13	17	10

Figure 2. Ablation of *Tis21* in *Patched1* heterozygous mice increases the frequency of mice with hyperplasia lesions as well as the number of lesions per cerebellum. ***A***, Representative images of lesions in cerebellar sagittal sections from Patched1 heterozygous mice, either *Tis21* wild-type ($Ptch1^{+/-}/Tis21^{WT}$/GFP) or *Tis21*-null ($Ptch1^{+/-}/Tis21^{KO}$/GFP) at 2, 6, and 12 weeks of age. Sections were stained with Hoechst 33258, and lesions were identified by the presence of GCPs expressing GFP, which is driven by the enhancer of Math1 in proliferating, normal and neoplastic, GCPs. Scale bar, 470 μm. ***B–D***, Percentage of mice with lesions (***B***), frequency of lesions per cerebellum (***C***), and volume of lesions (***D***) in $Ptch1^{+/-}/Tis21^{WT}$/GFP or $Ptch1^{+/-}/Tis21^{KO}$/GFP mice at 2, 6, and 12 weeks of age. ***E***, Number of mice analyzed in ***B–D***. *$p < 0.05$ or **$p < 0.01$, χ^2 test in ***B*** and Student's *t* test in ***C*** and ***D***. Error bars indicate SEM.

1 h pulse, did not change significantly in $Tis21^{KO}$ or in $Ptch1^{+/-}/Tis21^{KO}$ mice, compared with their respective controls (i.e., $Tis21^{WT}$ and $Ptch1^{+/-}/Tis21^{WT}$) (Fig. 4*A*,*B*). Similar results were obtained at P14 (Fig. 4*B*). This indicates that the absence of *Tis21* does not affect the proliferation rate of GCPs. Consistently, in GCPs isolated at P7, the absence of *Tis21* did not affect *cyclin D1* mRNA levels (Fig. 4*C*). This was unexpected, considering that Tis21 exerts an antiproliferative action through inhibition of *cyclin D1* when overexpressed in GCPs (Farioli-Vecchioli et al., 2007).

Next, we analyzed the differentiation of GCPs in the EGL by labeling GCPs with the neural markers NeuroD1 and NeuN at P7 and P14, respectively. NeuroD1 labels recently differentiated postmitotic GCPs of the inner EGL and is required for their differentiation (Miyata et al., 1999), while NeuN marks postmitotic differentiated granule neurons (Weyer and Schilling, 2003). At P7, the percentage of NeuroD1-positive GCPs in $Tis21^{KO}$ mice was significantly lower (25% decrease) than in $Tis21^{WT}$ mice; $Ptch1^{+/-}/Tis21^{KO}$ and $Ptch1^{+/-}/Tis21^{WT}$ mice presented equivalent percentages (Fig. 5*A*,*C*; $Tis21^{KO}$ vs $Tis21^{WT}$, $p < 0.0001$; $Ptch1^{+/-}/Tis21^{KO}$ vs $Ptch1^{+/-}/Tis21^{WT}$, $p = 0.1$). No differences between groups were observed in *NeuroD1* expression at P14 (Fig. 5*C*). However, the ablation of *Tis21* induced a decrease of GCPs positive for the late differentiation marker NeuN at P14, in both $Tis21^{KO}$ and $Ptch1^{+/-}/Tis21^{KO}$ mice, compared with their respective controls (i.e., $Tis21^{WT}$ and $Ptch1^{+/-}/Tis21^{WT}$) (Fig. 5*B*,*D*; $Tis21^{KO}$ vs $Tis21^{WT}$, and $Ptch1^{+/-}/Tis21^{KO}$ vs $Ptch1^{+/-}/Tis21^{WT}$, $p = 0.003$ and $p = 0.002$, respectively).

Together, these findings indicate that the ablation of *Tis21* can impair both the early and late differentiation.

Next, we measured the migration of GCPs from lesion-free areas of the EGL, by labeling them at P7 with a pulse of BrdU and analyzing their migration after 42 h or after 5 d. As shown in Figure 6, *A* and *C*, in *Tis21*-null mice ($Tis21^{KO}$ or $Ptch1^{+/-}/Tis21^{KO}$), a significantly lower percentage of BrdU-labeled GCPs migrated in the ML and in the IGL after 42 h (Fig. 6*A*,*C*; $Tis21^{KO}$ vs $Tis21^{WT}$, $p < 0.003$; or $Ptch1^{+/-}/Tis21^{KO}$ vs $Ptch1^{+/-}/Tis21^{WT}$, $p < 0.0001$; both in ML and IGL). Consistent with the reduced migration outside the EGL, an increase up to 1.5-fold of BrdU-labeled GCPs was observed in the EGL of $Tis21^{KO}$ mice, either *Patched1* wild-type or heterozygous (Fig. 6*A*,*C*; $Tis21^{KO}$ vs $Tis21^{WT}$, $p < 0.0001$; or $Ptch1^{+/-}/Tis21^{KO}$ vs $Ptch1^{+/-}/Tis21^{WT}$, $p < 0.0001$). The decreased migration of GCPs in the ML and IGL was specifically associated to the ablation of *Tis21*, as $Ptch1^{+/-}/Tis21^{WT}$ mice did not show any decrease in migration of GCPs when compared with $Tis21^{WT}$ (Fig. 6*C*; $p > 0.05$ in ML and IGL). Moreover, 5 d after labeling (at P12), the majority of BrdU-labeled GCPs had migrated outside the EGL in all groups, to reach their final destination, the IGL (Fig. 6*B*,*D*). However, in $Ptch1^{+/-}/Tis21^{KO}$ mice, a twofold higher percentage of GCPs

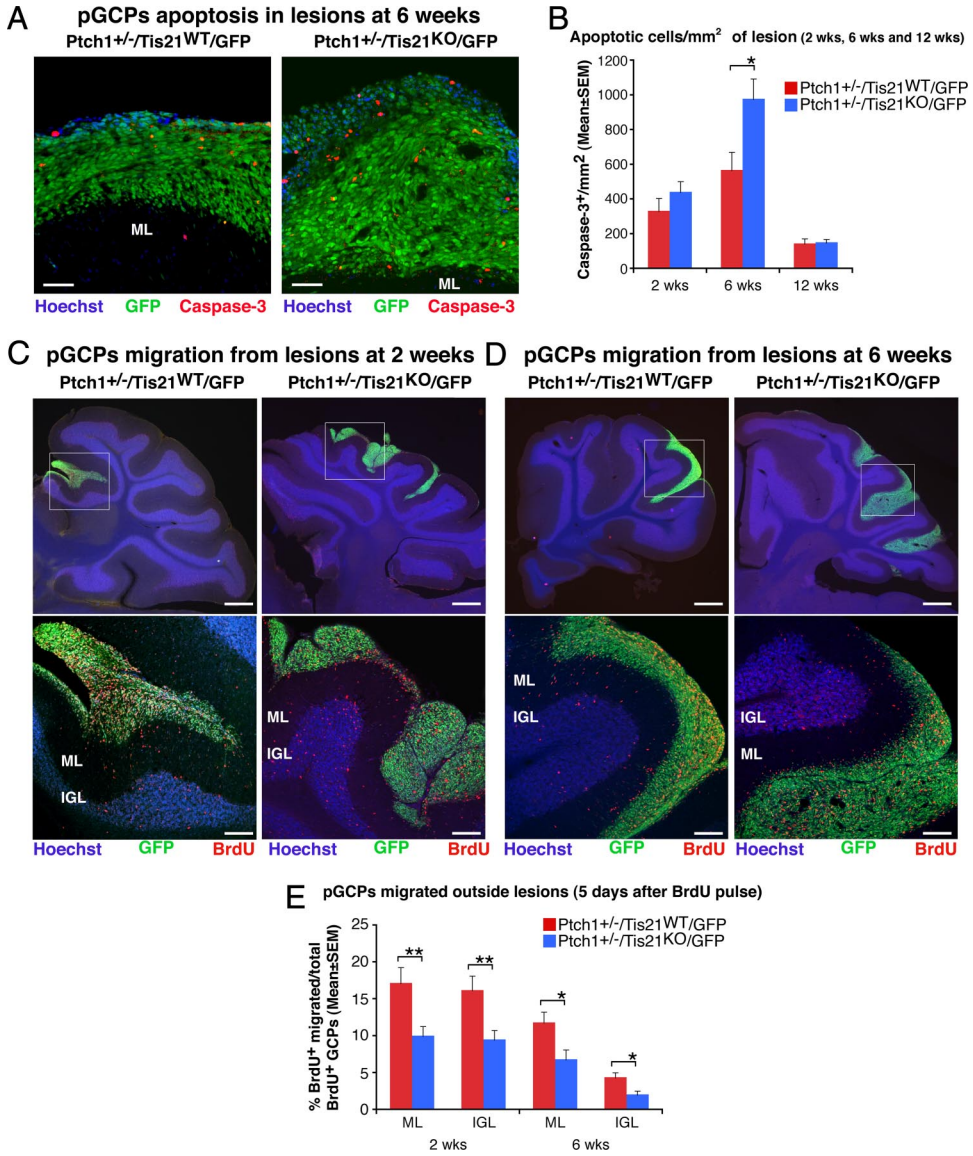

Figure 3. Ablation of *Tis21* in Patched1 heterozygous mice increases the apoptosis and impairs the migration from lesions of preneoplastic GCPs. ***A***, Representative confocal images of apoptotic GCPs, identified as cleaved Caspase-3-positive cells, in a diffuse hyperplasia lesion in *Patched1* heterozygous mice, either *Tis21* wild-type (*Ptch1*$^{+/-}$/*Tis21*^{WT}/GFP) or *Tis21*-null (*Ptch1*$^{+/-}$/*Tis21*^{KO}/GFP) at 6 weeks of age. Preneoplastic GCPs in the lesion are GFP^{+}; the ML and its boundaries are visualized by Hoechst 33258 staining. Scale bar, 50 μm. ***B***, Apoptotic GCPs per lesion area were quantified as mean ± SEM/mm^{2} of cleaved Caspase-3^{+} cells in the whole area of the lesion (defined by the presence of GFP^{+} cells), on at least five nonadjacent sagittal sections for each lesion. The number of mice analyzed is indicated in Figure 2 *E*. ***C***, ***D***, Representative confocal images of GCPs migrating outside the lesions, identified as BrdU^{+} cells (red), in *Patched1* heterozygous mice either *Tis21* wild-type (*Ptch1*$^{+/-}$/*Tis21*^{WT}/GFP) or *Tis21*-null (*Ptch1*$^{+/-}$/*Tis21*^{KO}/GFP) at 2 or 6 weeks of age. Sections are counterstained with Hoechst 33258 to visualize the ML or the IGL. Lesions in boxed area of top panels (scale bars, 410 μm) are shown at higher magnification in panels below (scale bars, 100 μm). ***E***, GCPs migrating from lesions were quantified as mean ± SEM percentage ratio of BrdU^{+} cells present within the ML or the IGL area neighboring each lesion 5 d after the BrdU pulse, to the total number of BrdU^{+} cells in lesion, ML and IGL. Three 2-week-old mice per genotype and at least four 6-week-old mice per genotype were analyzed. In ***B*** and ***E*** were analyzed all lesions present in each mouse cerebellum. *$p < 0.05$ or **$p < 0.01$, Student's *t* test.

was still present in the EGL and a lower percentage had migrated to the ML (Fig. 6*B*,*D*; *Ptch1*$^{+/-}$/*Tis21*^{KO} vs *Ptch1*$^{+/-}$/*Tis21*^{WT}, $p = 0.02$ in ML), suggesting that the defect in migration persisted longer if the mutation of *Tis21* was associated with that of *Patched1*. Furthermore, we found no defect in *Tis21*-null mice, either Patched1 wild-type or heterozygous, in the organization of the Bergmann radial glia, detected by GFAP, which guides granule cell migration (Hatten, 1999) (data not shown).

We also evaluated the survival of GCPs in the EGL at P7 and P14, and found no significant changes in the percentage of GCPs undergoing apoptosis between the four different genotypes studied, as detected by positivity to cleaved Caspase-3 (data not shown).

As the ablation of *Tis21* caused a defective migration of GCPs evident not only in EGL but also in hyperplastic lesions, while differentiation in lesions was normal, we decided to further investigate the migration of GCPs by analyzing organotypic cerebellar slice cultures.

Indeed, a defective migration out of the EGL was observed in BrdU-positive GCPs of organotypic slices from *Tis21*-null mice, either *Patched1* wild-type or heterozygous, compared with *Tis21* wild-type mice (Fig. 7*A*,*B*; *Tis21*^{KO} vs *Tis21*^{WT}, or *Ptch1*$^{+/-}$/*Tis21*^{KO} vs *Ptch1*$^{+/-}$/*Tis21*^{WT}, $p < 0.0001$).

We further sought to test whether, either in the presence or in the absence of activated *Shh* signaling, GCPs lacking *Tis21* presented a migration defect per se. To this aim, we analyzed the ability of puri-

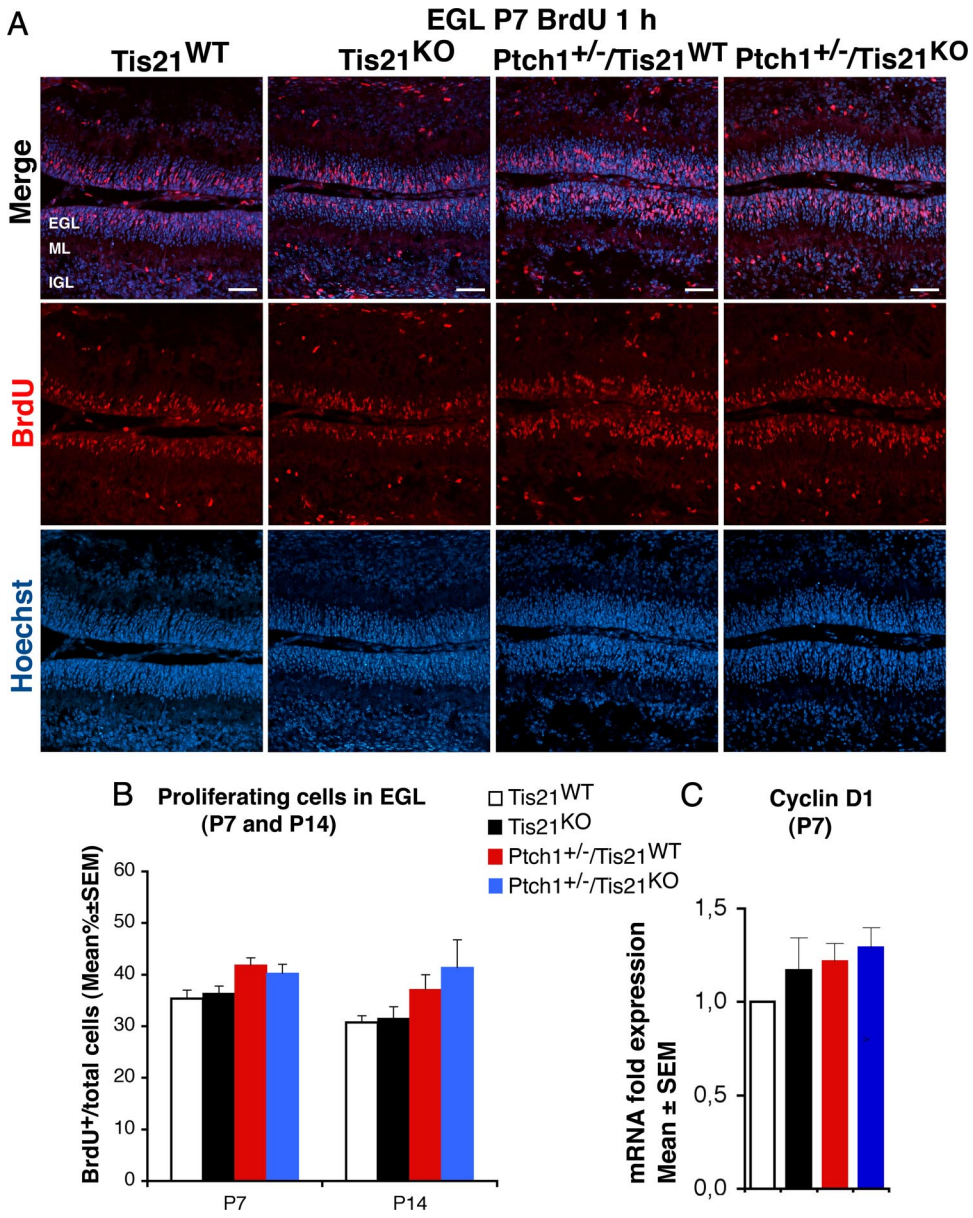

Figure 4. Ablation of *Tis21* in *Patched1* heterozygous or wild-type mice does not influence the proliferation of GCPs in the EGL. ***A***, Representative confocal images of GCPs in the EGL of P7 mice of the four genotypes indicated, entering in the cell cycle S-phase, identified as BrdU-positive cells after a short pulse of BrdU (1 h). Sections are counterstained with Hoechst 33258 to visualize the EGL and the granule neurons and precursors contained. Scale bar, 50 μm. ***B***, Quantitative analysis in the EGL of P7 or P14 mice with the indicated genotype, of GCPs that have entered the S-phase of cell cycle, measured as mean ± SEM percentage ratio between the number of BrdU$^+$ cells and the total number of cells (labeled by Hoechst 33258; BrdU labeling index). Three mice for each genotype were analyzed. ***C***, Real-time PCR analysis in isolated GCPs from P7 mice of mRNA fold expression relative to wild-type mice (set to unity). Mean ± SEM fold increases are from three independent experiments. *TBP* and *GAPDH* were used to normalize data.

fied GCPs—isolated at P7 as GFP$^+$ cells by FACS—to migrate in a modified Boyden chamber, as previously described (Lu et al., 2001). Briefly, a membrane filter with uniform pore size divides upper and lower chambers. GCPs are seeded in the upper chamber, and the number of those that have migrated to the lower surface of the filter is determined. The number of *Ptch1*$^{+/-}$/*Tis21*^{KO}/GFP double-mutant GCPs that migrated to the lower chamber was significantly lower than that of *Ptch1*$^{+/-}$/*Tis21*^{WT}/GFP GCPs (Fig. 7*C*; 32% decrease; $p < 0.0001$). A quantitatively similar decrease of migration was observed also in GCPs of *Tis21*-null *Patched1* wild-type mice (Fig. 7*C*; *Tis21*^{KO}/GFP vs *Tis21*^{WT}/GFP; $p < 0.0001$). This indicates that the ablation of *Tis21* has an effect on the intrinsic ability of GCPs to migrate, both in the presence or absence of activated *Shh* signaling.

Moreover, when we infected organotypic cerebellar slices from *Tis21*-null mice, either Patched1 wild-type or heterozygous, with a retrovirus expressing *Tis21* and the Tomato red fluorescent protein, the defective migration of GCPs was significantly rescued (Fig. 7*D–G*; Tomato-Tis21$^+$ vs Tomato-empty$^+$ in *Tis21*^{KO} mice, $p = 0.02$; Tomato-Tis21$^+$ vs Tomato-empty$^+$ in *Ptch1*$^{+/-}$/*Tis21*^{KO} mice, $p = 0.003$). This indicates that the defect of migration is reversible and specifically dependent on the loss of *Tis21*.

Tis21 knock-out/medulloblastoma-specific gene expression

To start investigating the molecular mechanisms underlying the complex phenotype observed in *Tis21*-null cerebellum, by real-time PCR we analyzed the expression levels of components of three main pathways known to regulate migration of cerebellar

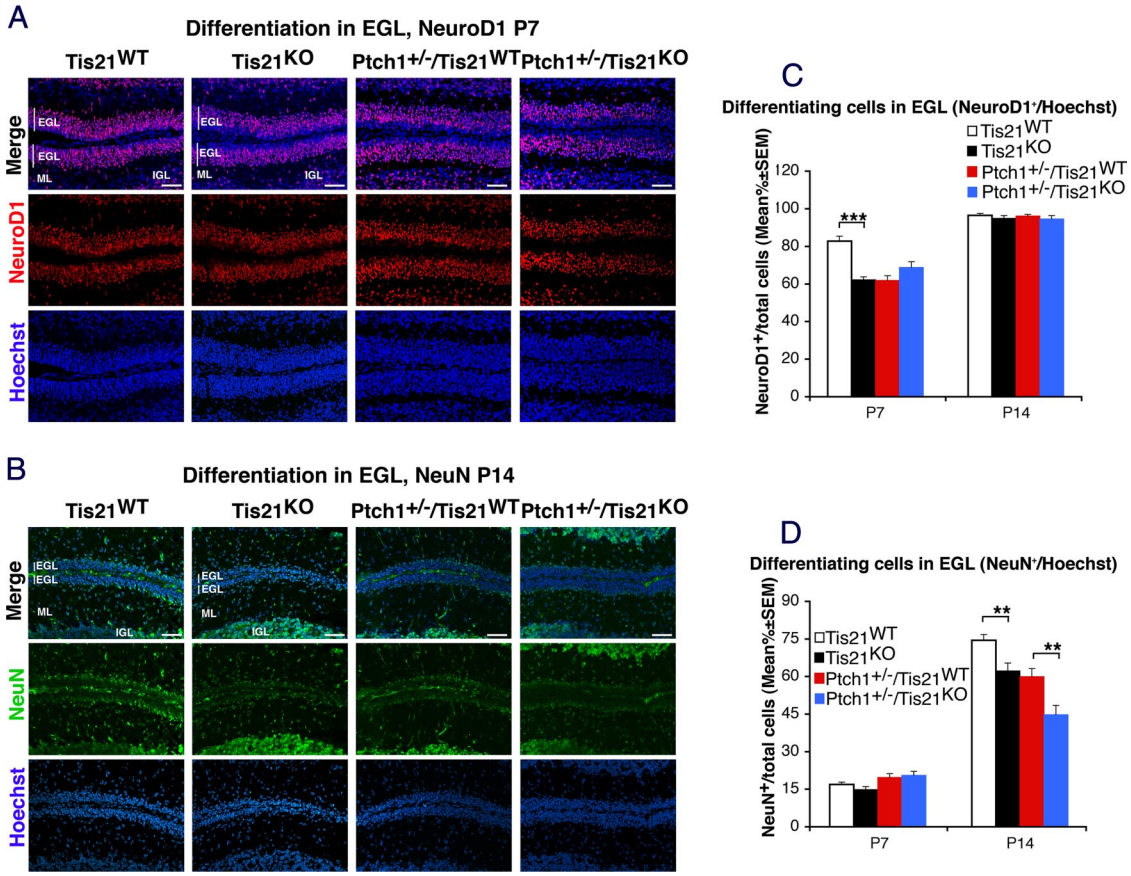

Figure 5. Ablation of *Tis21* in *Patched1* heterozygous or wild-type mice reduces the differentiation of GCPs in the EGL. ***A***, ***B***, Representative confocal images of GCPs in the EGL of the four genotypes indicated; NeuroD1 expression in P7 mice (***A***) and NeuN expression in P14 mice (***B***). Sections are counterstained with Hoechst 33258 to visualize the EGL and the ML and IGL. Scale bar: 50 μm. ***C***, ***D***, Quantitative analysis of GCPs expressing NeuroD1 in the EGL of P7 and P14 mice (***C***) or expressing NeuN (***D***), represented as mean ± SEM percentage ratio between the number of NeuroD1$^+$ or NeuN$^+$ cells, respectively, and the total number of cells (labeled by Hoechst 33258) ($n = 3$ for each genotype). $^{**}p < 0.01$ or $^{***}p < 0.001$, Student's *t* test.

neurons, namely *BDNF* and its receptor *TrkB* (Borghesani et al., 2002; Kokubo et al., 2009), *astrotactin1/astrotactin2* (Wilson et al., 2010), and *neuregulin* and its receptor *Erb4* (Rio et al., 1997). However, we could not detect significant changes of these mRNAs in GCPs isolated from P7 mice, either double mutant or *Patched1* wild-type/*Tis21*-null, compared with the respective *Tis21* wild-type controls (data not shown). Therefore, we performed a genome-wide mRNA analysis by microarray in GCPs isolated from the EGL of P7 mice. We compared gene expression between *Tis21*-null and *Tis21* wild-type mice, either in *Patched1* wild-type background ($Tis21^{KO}$ vs $Tis21^{WT}$) or in *Patched1* heterozygous background ($Ptch1^{+/-}/Tis21^{KO}$ vs $Ptch1^{+/-}/Tis21^{WT}$). We assumed that genes whose expression was significantly modified only in the first comparison may be related to *Tis21* knock-out non-tumor-specific cerebellar phenotypes, while genes significantly modified in the second comparison (or in both comparisons) may be specifically involved in the *Tis21* knock-out-dependent enhancement of medulloblastoma formation. In this way, we identified 344 differentially expressed genes, of which 179 were *Tis21* knock-out-specific and 165 medulloblastoma-specific (Fig. 8*A*,*B*). A comprehensive picture of these transcriptional changes is shown with a hierarchical clustering method (Fig. 8*B*), in which the 344 genes are grouped on the basis of similarity in their expression patterns. Among these, we identified 11 *Tis21* knock-out-specific and 22 medulloblastoma-specific genes known to be involved in the processes of migration, neurogenesis, differentiation, or cell adhesion and motility, as defined by gene ontology annotations (Fig. 8*C*,*D*). Among the 22 medulloblastoma-specific genes, 5 of them showed concordant expression changes also in Patched1 wild-type background ($Tis21^{KO}$ vs $Tis21^{WT}$) and have been previously associated to the neuronal phenotype. These genes are the chemokines *Cxcl3* and *Cxcl12* (de Haas et al., 2007), *Pag1* (Feng et al., 2009; Georgakopoulos et al., 2011), *Efna4* (Wilkinson, 2001), and *Jmy* (Coutts et al., 2009; Zuchero et al., 2009). Their expression changes were validated by real-time PCR in GCPs from the EGL of P7 mice (Fig. 8*E*). All these genes showed significantly different expression in double-mutant mice compared with *Patched1* heterozygous mice, thus matching the microarray results, with *Cxcl3* showing the highest decrease (~45%; $Ptch1^{+/-}/Tis21^{KO}$ vs $Ptch1^{+/-}/Tis21^{WT}$, $p = 0.003$). Remarkably, in pGCPs isolated from diffused lesions in 6-week-old double-mutant mice as GFP$^+$ cells by FACS, *Cxcl3* expression almost disappeared (95% decrease; $p = 0.0007$; Fig. 8*E*), while the other genes did not differ (data not shown).

Cxcl3 counteracts the GCPs migration defect and reduces the lesion area

To investigate the functional implications of *Cxcl3* downregulation, we tested the ability of *Cxcl3* to revert the defective migration of *Tis21*-null GCPs. To this end, we treated organotypic cerebellar slices from *Tis21*-null mice at P7, either Patched1 wild-type or heterozygous, with the Cxcl3 recombinant protein for 5 d. We observed that Cxcl3 significantly neutralized the defect of migration of GCPs from the EGL, as indicated by the percentage of BrdU$^+$ GCPs migrated out of EGL (Fig. 9*A*,*B*; with Cxcl3 vs

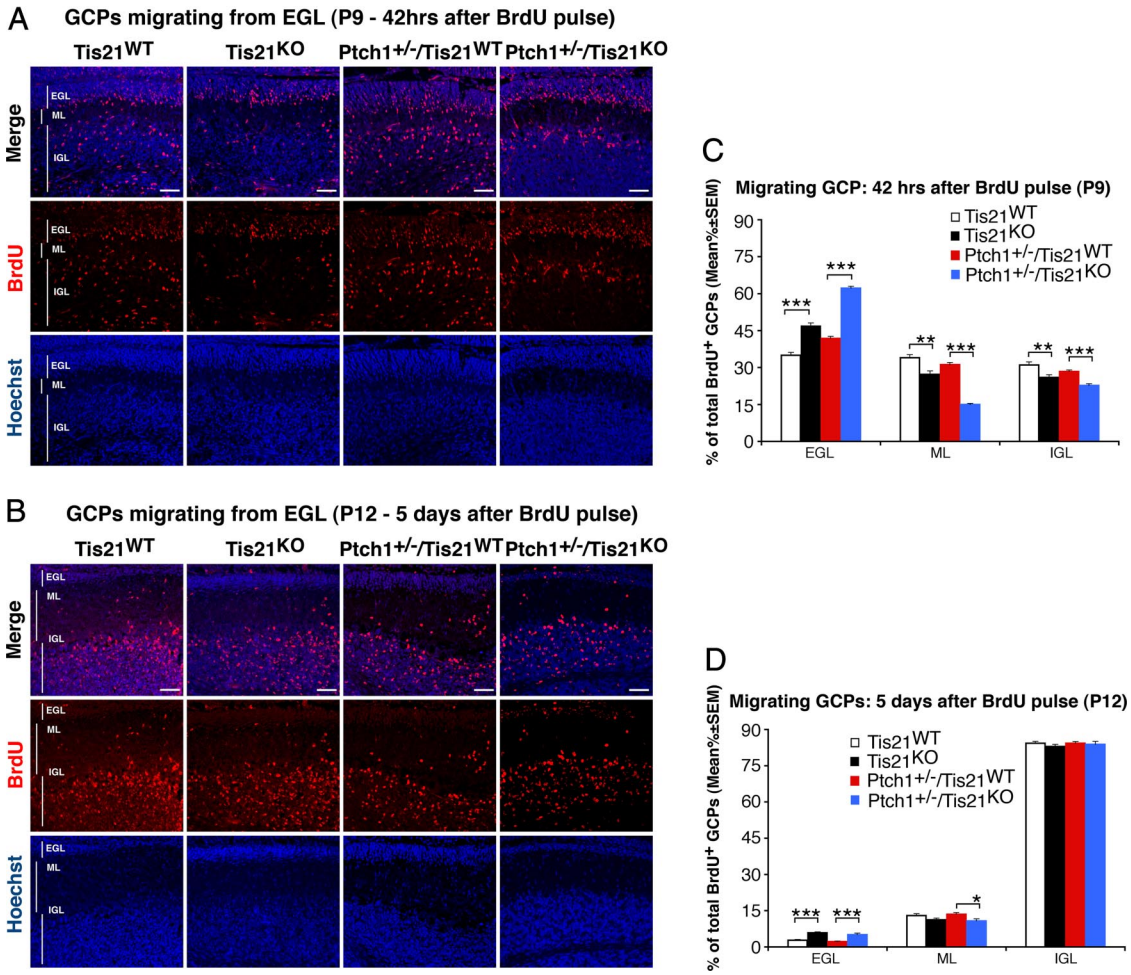

Figure 6. Ablation of *Tis21* in *Patched1* heterozygous or wild-type mice impairs the migration of GCPs from EGL to molecular and internal granular layers. ***A***, ***B***, Representative confocal images of GCPs migrating outside the EGL, identified as BrdU $^+$ cells in *Tis21*-null and wild-type mice, in either *Patched1* heterozygous or wild-type background, as indicated. P7 mice were injected with BrdU and analyzed after 42 h (***A***) or after 5 d (***B***). Sections are counterstained with Hoechst 33258 to visualize the ML and the IGL. Scale bars, 50 μm. ***C***, ***D***, Quantification of GCPs migrating from the EGL 42 h after BrdU injection in P7 mice (***C***), or after 5 d (***D***), represented as mean ± SEM percentage ratio of BrdU $^+$ cells in the EGL, ML, or IGL to the total BrdU $^+$ cells. Three mice per genotype were analyzed. *$p < 0.05$, or **$p < 0.01$, or ***$p < 0.001$, Student's *t* test.

without: in $Tis21^{KO}$ mice, $p = 0.001$, or in $Ptch1^{+/-}/Tis21^{KO}$ mice, $p < 0.0001$). In particular, in double-mutant mice, Cxcl3 induced ~75% of GCPs to migrate outside the EGL (i.e., nearly attaining the basal level of migration observed in wild-type mice) (Fig. 7*B*). Additionally, we checked whether Cxcl3 treatment affected the proliferation or differentiation of GCPs, by analyzing them in the EGL of cerebellar slices obtained from P7 mice of the four genotypes under study, exposed to the Cxcl3 protein for 48 h. GCPs treated with Cxcl3 did not present significant differences of proliferation, as defined by the percentage of BrdU $^+$ cells after a 2 h pulse, or differentiation (NeuroD1 $^+$ and NeuN $^+$ cells), relative to untreated control slices (Fig. 9*C*). We further sought to test whether the positive effect of Cxcl3 on the migration of GCPs was cell autonomous or whether it was indirect. To this aim, we silenced *Cxcl3* in preparations of purified GCPs from P7 wild-type rats, by transfecting two specific siRNAs interacting with *Cxcl3* mRNA, siRNA7-*Cxcl3* or siRNA6-*Cxcl3*. These were selected between several 19 nt candidate sequences targeting *Cxcl3* designed by the MWG Design Tool software (MWG), as sequences capable to reduce the levels of Cxcl3 mRNA, relative to control GCPs transfected with a control siRNA targeting the luciferase gene (Fig. 9*D*, right; siRNA7-*Cxcl3*, $p = 0.0001$; siRNA6-*Cxcl3*, $p = 0.002$). A significantly lower number of GCPs transfected with either siRNA7-*Cxcl3* or siRNA6-*Cxcl3* were able to migrate to the lower part of a modified Boyden chamber, compared with GCPs transfected with siRNA-control (Fig. 9*D*, left; $p = 0.002$ or $p = 0.006$, respectively). A parallel analysis of the state of differentiation of the same preparations of GCPs, either silenced for Cxcl3 or control, did not show differences in the percentage of expression of NeuN (63.8 ± 2.2 for GCPs transfected by siRNA7-*Cxcl3*, 61.9 ± 1.1 for siRNA6-*Cxcl3*, and 62.9 ± 3.2 for siRNA-control; three independent experiments of isolation and transfection of GCPs). Similarly, cerebellar slices from P7 wild-type mouse transfected with siRNA6-*Cxcl3* presented a lower number of GCPs migrated out of EGL, relative to GCPs transfected with siRNA-control (data not shown). Therefore, these data indicate that Cxcl3 plays a cell-autonomous role required in the migration of the GCPs out of the EGL.

Having ascertained this, we further analyzed the effect of Cxcl3 on GCPs within lesions. Remarkably, at P30, 5 d of treatment with Cxcl3 significantly reduced the area of lesions in slices (Fig. 9*E*,*F*; Cxcl3 day 0 vs day 5, in $Ptch1^{+/-}/Tis21^{KO}$/GFP mice, $p = 0.003$) and, correspondingly, significantly reversed the defect of migration of pGCPs (labeled by BrdU $^+$) outside lesions (Fig. 9*E*,*G*; with Cxcl3 vs without, in $Ptch1^{+/-}/Tis21^{KO}$/GFP mice,

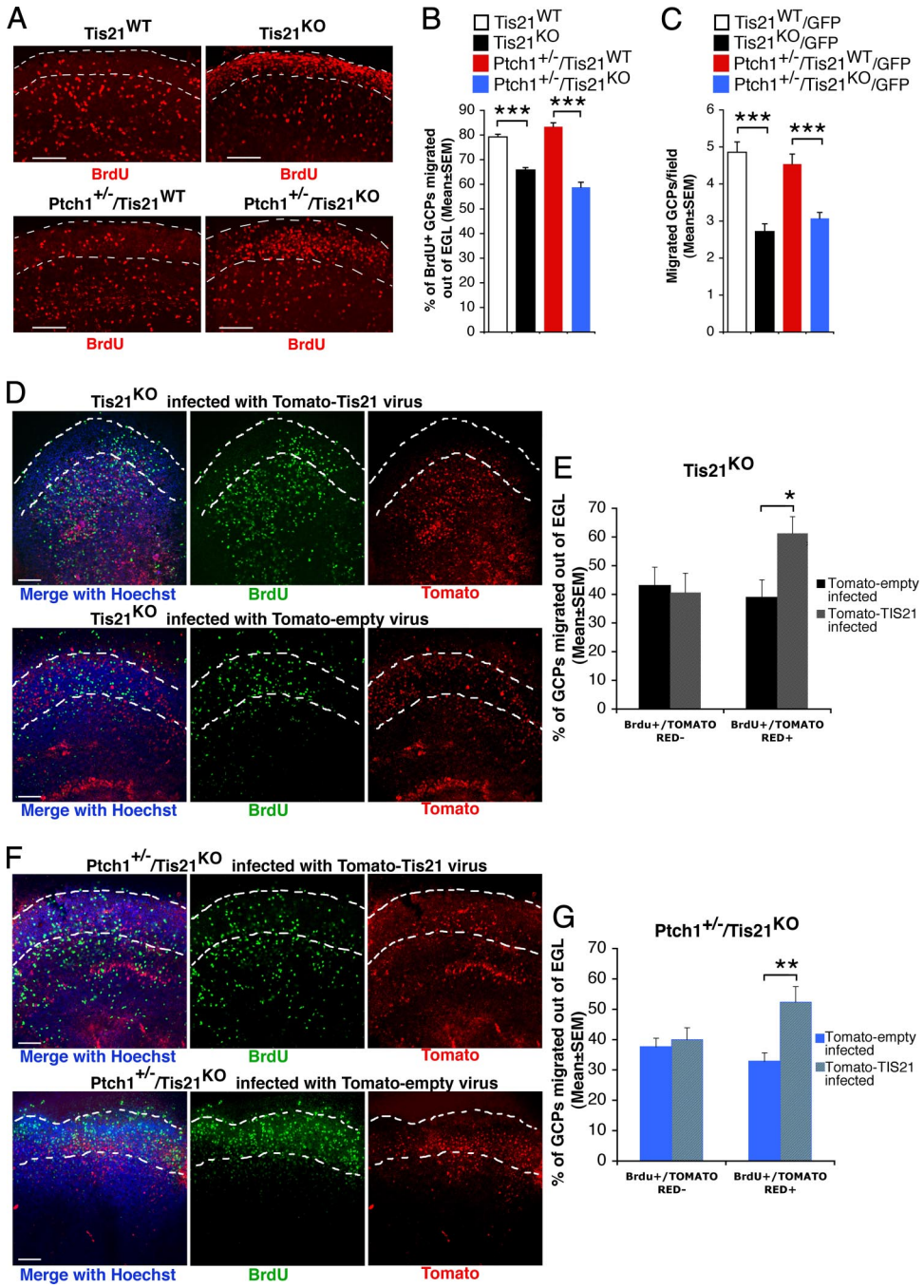

Figure 7. The impairment of migration of GCPs outside the EGL in *Tis21* knock-out mice is rescued in organotypic slices by *Tis21*. ***A***, Representative confocal images of cerebellar organotypic slices, showing BrdU $^+$ GCPs inside or outside the EGL (whose boundaries are indicated by a white broken line). Slices, obtained from P7 mice of the indicated genotype, were pulse-labeled with BrdU for 6 h, cultured for additional 72 h, fixed, and immunostained with anti-BrdU antibody. Scale bars, 100 μm. ***B***, Percentage ratio between BrdU-positive cells localized outside the EGL, and the total number of BrdU-positive cells. Data are mean ± SEM from three experiments (3 mice per genotype were analyzed). ***$p < 0.001$, Student's *t* test. ***C***, Test by a modified Boyden chamber of the intrinsic ability of purified GCPs to migrate. GFP $^+$ GCPs isolated by FACS from P7 cerebellum of GFP mice (of the indicated genotype) were placed in the upper chamber, and cells migrating to the lower side of the membrane were counted. Mean cell number per field ± SEM were obtained from three separate experiments, counting 20 fields per well (at least 2 wells per experiment). The number of migrated *Tis21*-null GCPs, either Patched1 wild-type or heterozygous, was significantly reduced with respect to *Tis21* wild-type GCPs. ***$p < 0.01$, Student's *t* test. ***D–G***, In cerebellar slices, *Tis21*-retrovirus rescues the defective migration of *Tis21*-null GCPs. ***D***, ***F***, Representative confocal images of cerebellar slices, showing BrdU $^+$ and Tomato-Tis21 $^+$ or Tomato-empty $^+$ GCPs inside or outside the EGL. Slices, obtained from P7 *Tis21* knock-out mice in Patched1 background, either *Tis21*^{KO} (***D***) or *Ptch1*$^{+/-}$/*Tis21*^{KO} (***F***), were infected with Tomato-*Tis21* or Tomato-empty retrovirus, pulse-labeled with BrdU for 6 h, cultured for additional 72 h, fixed, and immunostained with anti-BrdU antibody. Scale bars, 100 μm. ***E***, ***G***, The percentage ratio between BrdU $^+$/Tomato $^+$ or BrdU $^+$/Tomato $^-$ cells outside the EGL, and the total number of BrdU $^+$ cells was analyzed in slices from either *Tis21*^{KO} (***E***) or *Ptch1*$^{+/-}$/*Tis21*^{KO} mice (***G***), infected with Tomato-*Tis21* or Tomato-empty retrovirus. The absence of effect in BrdU $^+$/Tomato $^-$ cells is a control of the specificity of infection. Data are mean ± SEM from three experiments (3 mice per genotype were analyzed). *$p < 0.05$, or **$p < 0.01$, Student's *t* test.

$p = 0.0006$). This indicates that the addition of exogenous Cxcl3 can rescue the *Tis21*-dependent defect of migration of GCPs also at a preneoplastic stage within lesions and, in consequence of this, reduces the area of lesions.

Tis21 is recruited to the *Cxcl3* promoter and induces its activity

The above data indicate that *Cxcl3* plays a central role in the migration of normal and preneoplastic GCPs and that its expres-

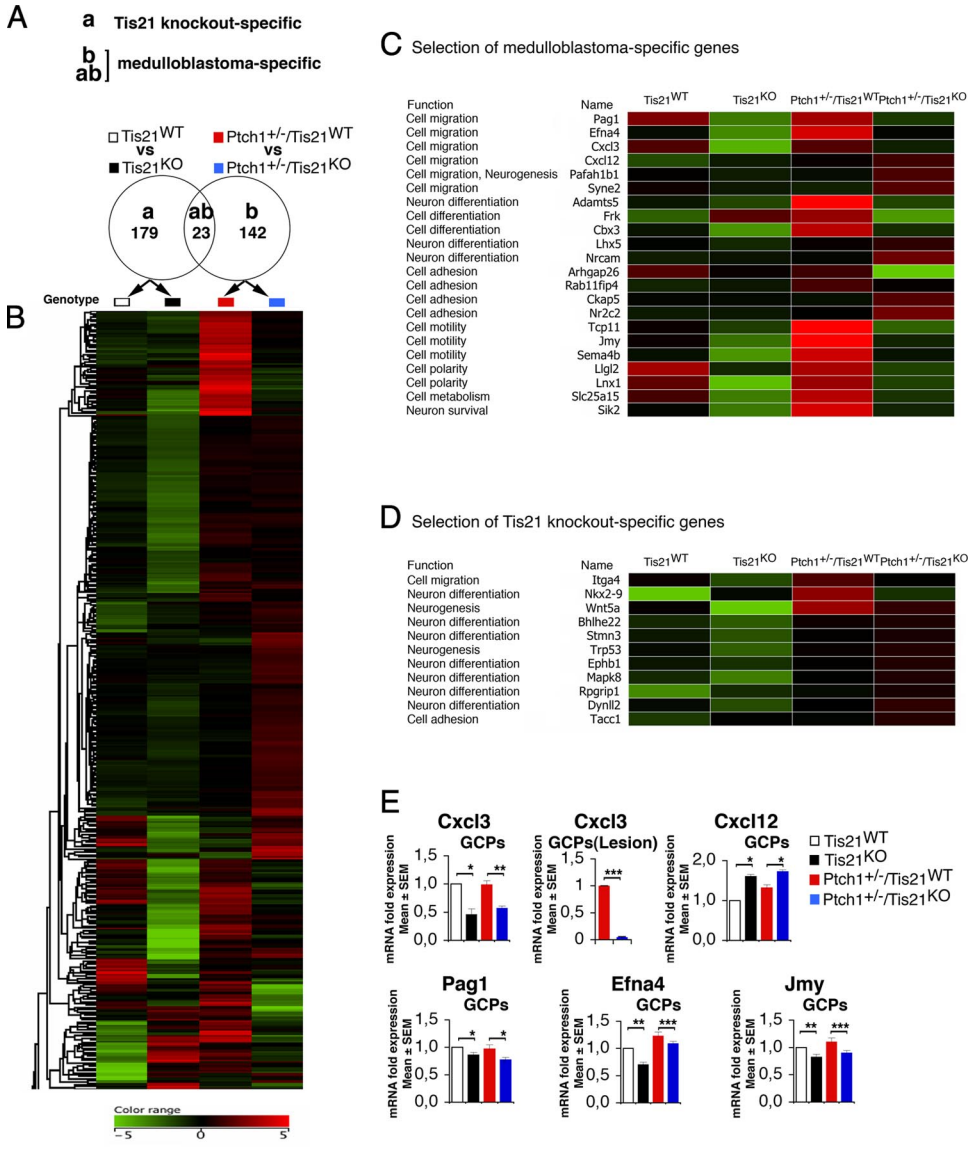

Figure 8. Medulloblastoma-specific gene expression in *Patched1* heterozygous/*Tis21*-null model. ***A***, As shown in the Venn diagram, microarray analysis of GCPs in P7 mice identified 179 *Tis21* knock-out-specific genes, whose expression significantly differed only in pairwise comparison (a): *Patched1* wild-type/*Tis21*-null versus wild type ($Tis21^{KO}$ vs $Tis21^{WT}$). Likewise, 165 medulloblastoma-specific genes were identified whose expression significantly differed in pairwise comparison (b): *Patched1* heterozygous/*Tis21*-null versus *Patched1* heterozygous/*Tis21* wild-type ($Ptch1^{+/-}/Tis21^{KO}$ vs $Ptch1^{+/-}/Tis21^{WT}$). Twenty-three genes significantly differed in both comparisons (a) and (b). ***B***, A hierarchical clustering algorithm (similarity measure, euclidean; linkage rule, centroid) was used to order the 344 genes differentially expressed in both pairwise comparisons (a) and (b). Colors indicate high expression (red) to low expression (green), corresponding to changes of normalized values relative to the median value. ***C***, Twenty-two medulloblastoma-specific genes are involved in cell migration, differentiation, or adhesion processes. ***D***, Eleven *Tis21* knock-out-specific genes are involved in cell migration or differentiation processes. ***E***, The differential expression of five neuronal medulloblastoma-specific genes in GCPs from the EGL at P7 or from lesions (GFP^{+}) at 6 weeks was confirmed by real-time PCR, analyzing mRNA fold expression relative to wild-type mice (set to unity). Mean ± SEM fold increases are from three independent experiments. *TBP* and *GAPDH* were used to normalize data. $*p < 0.05$, $**p < 0.01$, or $***p < 0.001$, Student's *t* test.

sion is controlled by *Tis21*. Given that *Tis21* is a transcriptional cofactor known to be recruited to the promoter of *cyclin D1*, *Id3*, and *RAR-β* (Passeri et al., 2006; Farioli-Vecchioli et al., 2007, 2009), we sought to define whether *Tis21* directly controls the transcription of *Cxcl3*. First, we determined the effect of *Tis21* overexpression on *Cxcl3* mRNA levels in primary cultures of postmitotic cerebellar granule neurons from P7 wild-type rats, infected with adenoviruses expressing either *Tis21* (rat sequence) or β-Gal. As shown in Figure 10, *A* and *B*, the expression of exogenous Tis21 in cerebellar granule neurons was associated with a corresponding increase of the levels of *Cxcl3* mRNA, relative to control ($p = 0.012$; Fig. 10*B*).

We further sought to check whether the upregulation of *Cxcl3* mRNA elicited in cerebellar granule neurons by overexpression of Tis21 corresponded to an induction of *Cxcl3* promoter activity. Therefore, we generated the construct pGL3-*Cxcl3*-prom/-628, carrying the *Cxcl3* promoter region upstream of the luciferase reporter gene. This construct was either cotransfected into cerebellar granule neurons together with a *Tis21*-expressing vector (pSCT-*Tis21*), or transfected in PC12 cells expressing an inducible *Tis21* gene (rat sequence) under control of the tetracycline-regulatable tTA transactivator (PC12/tetoff) (Farioli-Vecchioli et al., 2009). *Cxcl3* promoter activity was significantly induced in both cerebellar granule neurons and PC12 cells expressing *Tis21*, relative to the corresponding con-

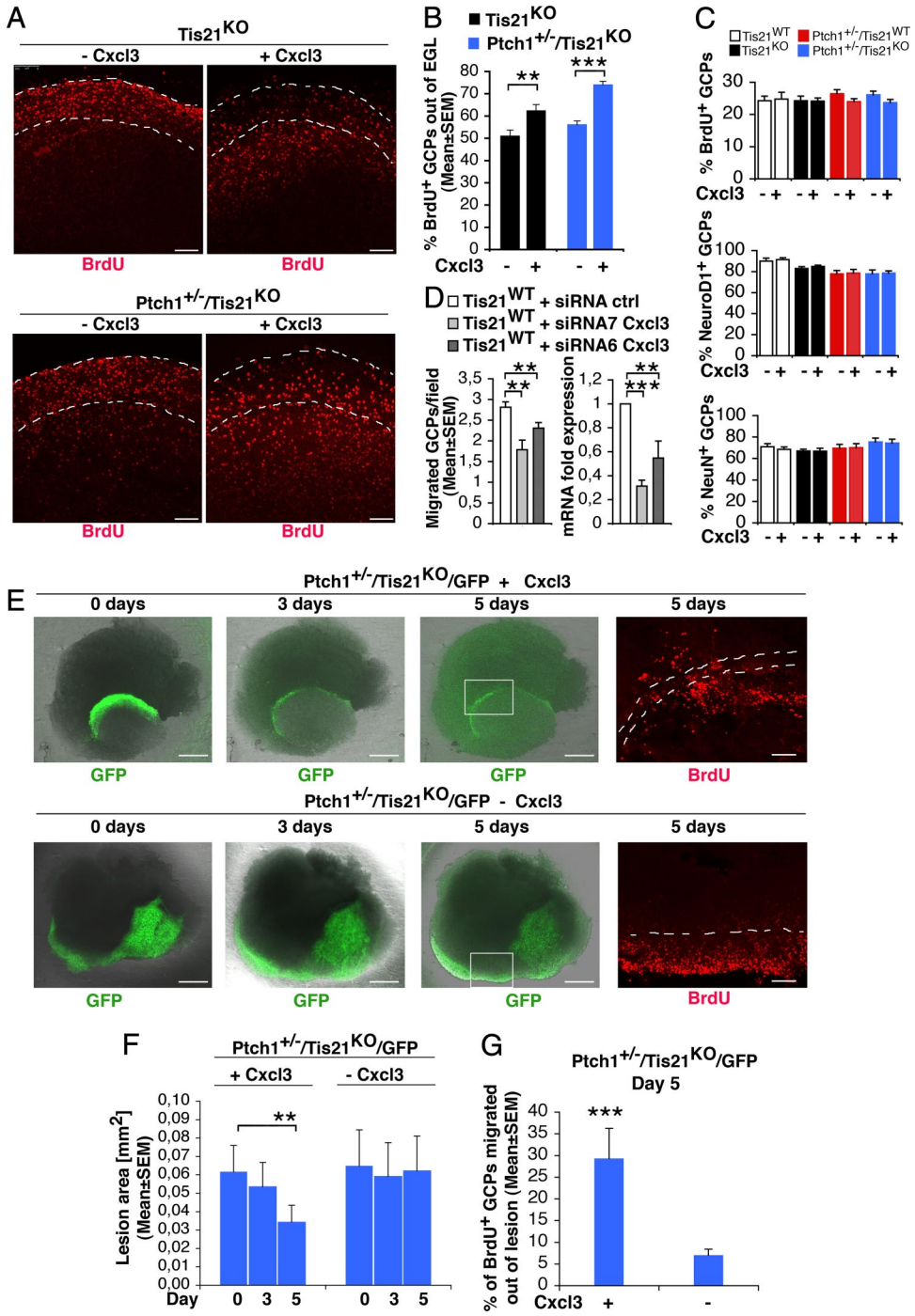

Figure 9. Cxcl3 rescues the defective migration of GCPs outside the EGL or outside lesions, and reduces the area of lesions in *Patched1* heterozygous/*Tis21* knock-out mice. ***A***, Representative confocal images of cerebellar organotypic slices from *Tis21*-null/*Patched1* wild-type or heterozygous mice treated with or without Cxcl3, showing BrdU $^+$ GCPs inside or outside the EGL (indicated by a white broken line). Scale bars, 100 μm. ***B***, Quantification of BrdU $^+$ GCPs migrated outside the EGL. Slices from P7 mice were cultured 5 d with or without Cxcl3 (adding BrdU at t0 for 18 h), fixed, and immunostained with anti-BrdU antibody. Shown is the mean $\pm$ SEM percentage ratio between BrdU-positive cells outside EGL and total number of BrdU-positive cells (from 3 experiments; 3 mice per genotype were analyzed). $^{**}p < 0.01$ or $^{***}p < 0.001$, Student's *t* test. ***C***, Quantification of proliferating (BrdU $^+$) or differentiating (NeuroD1 $^+$ or NeuN $^+$) GCPs in the EGL after treatment with Cxcl3. Slices from P7 mice were cultured 48 h with or without Cxcl3 (adding BrdU 2 h before analysis), fixed, and immunostained with antibodies against BrdU, NeuroD1, or NeuN (mean $\pm$ SEM percentage ratio between BrdU $^+$, NeuroD1 $^+$, or NeuN $^+$ cells in the EGL and total number of cells, from 3 experiments; 3 mice per genotype were analyzed). ***D***, RNAi knockdown of *Cxcl3* in GCPs leads to inhibition of their ability to migrate (graph on the left). Purified GCPs from wild-type P7 rat cerebella were transfected by electroporation with siRNAs targeting *Cxcl3* (either siRNA7-*Cxcl3* or siRNA6-*Cxcl3*) or with a control siRNA; immediately thereafter, GCPs were seeded (6×10^6) onto 35 mm dishes in recovery medium (with high serum) for 3 h, and then transferred in the upper part of a modified Boyden chamber. After 16 h, the GCPs migrating to the lower side of the membrane were counted. Mean cell number per field $\pm$ SEM were obtained from three separate experiments, counting 20 fields per well (at least 2 wells per experiment). The graph on the right shows the levels of *Cxcl3* mRNA in the same preparations of purified GCPs transfected for migration tests (mean $\pm$ SEM fold increases; TBP was used to normalize data). $^{**}p < 0.01$, $^{***}p < 0.001$, Student's *t* test. ***E***, Representative confocal images of diffuse hyperplasia lesions in cerebellar organotypic slices treated with or without Cxcl3, from *Patched1* heterozygous/*Tis21*-null mice (*Ptch1*$^{+/-}$/*Tis21*^{KO}/GFP) at 4 weeks of age, showing GFP $^+$ GCPs inside the lesion (green), and a magnification of BrdU $^+$ GCPs (red) migrating outside lesions (bordered by white broken line) in the presence or absence of Cxcl3. Scale bars: 500 or 100 μm for GFP or BrdU panels, respectively. ***F***, ***G***, Quantification of lesion area (***F***) and percentage of BrdU $^+$ GCPs migrated outside the lesion (***G***). Slices obtained from P42 mice were treated with Cxcl3 for 5 d and pulse-labeled with BrdU added at t0 for 18 h, fixed, and immunostained with anti-BrdU antibody. Data are mean $\pm$ SEM from three experiments (3 mice per genotype were analyzed). $^{**}p < 0.01$ or $^{***}p < 0.001$, Student's *t* test.

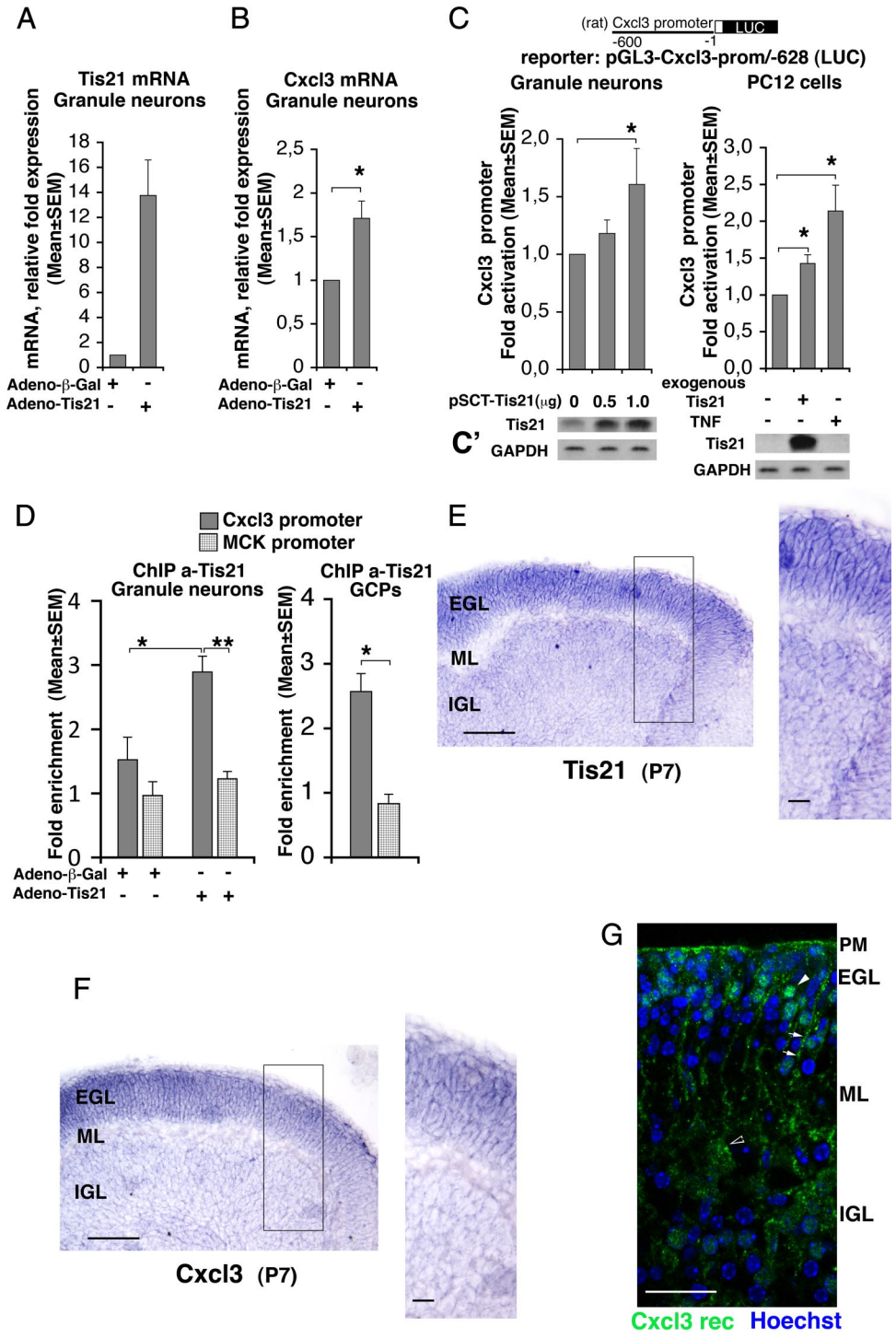

Figure 10. Tis21 associates to the *Cxcl3* promoter and induces *Cxcl3* transcription. ***A***, ***B***, Real-time RT-PCR analysis of *Tis21* and *Cxcl3* mRNAs in primary cultures of cerebellar granule neurons. Cells, obtained from P7 rats, were plated and infected with recombinant adenoviruses adeno-*Tis21* or control adeno-*β-Gal* the same day of plating (DIV 0), and harvested after 24 h. The primers amplifying *Tis21* (rat sequence) detected both the endogenous and exogenous mRNA. Shown are mean ± SEM values are from five separate experiments. TATA-binding protein mRNA was used as endogenous control for normalization. $*p < 0.05$ versus control, Student's *t* test (performed on data normalized to the endogenous controls but not yet relativized as fold expression). ***C***, *Cxcl3* promoter activity in cerebellar granule neurons from P7 wild-type rats transfected with an expression vector for *Tis21* (pSCT-*Tis21*) and in PC12 cells expressing inducible Tis21 (rat sequence) increased significantly, relative to the corresponding controls expressing endogenous levels of Tis21. The *Cxcl3* promoter construct comprises 628 nt 5′ to the putative transcription start, placed upstream of a luciferase reporter (construct pGL3-*Cxcl3*-prom/-628). TNF-α, known inducer of *Cxcl3* promoter activity, is used in PC12 cells as positive control. Luciferase activity is represented as mean ± SEM fold increase from five separate experiments. $*p < 0.05$ versus the corresponding control without exogenous or ectopic Tis21, Student's *t* test. ***C'***, Parallel cultures were analyzed for Tis21 protein expression by Western blot. ***D***, ChIP analysis of Tis21 binding to the *Cxcl3* promoter and to the *muscle creatine kinase* promoter (*MCK*) (negative control) either in cerebellar granule neurons (graph on the left), infected with adeno-*Tis21* or adeno-*β-Gal* as in ***A*** and ***B***, or in GCPs (graph on the right), both isolated from P7 wild-type rats. The amount of *Cxcl3* or *MCK* promoters present in immunoprecipitates, obtained using anti-Tis21 antibody A3H, is quantified by real-time PCR and is expressed as fold enrichment (ratio of the percentage of the Tis21-immunoprecipitated amount of *Cxcl3* or *MCK* promoter detected in the input cell lysates to the percentage of the normal serum-immunoprecipitated amount detected in the input cell lysates). The binding of Tis21 protein to the *Cxcl3* promoter (darker gray columns) significantly increases above basal levels (i.e., above the binding levels to the *MCK* negative control promoter) in correlation with the overexpression of *Tis21* mRNA (compare also ***A***). Shown are mean ± SEM values are from five separate experiments performed with cerebellar granule neurons and from three separate (*Figure legend continues.*)

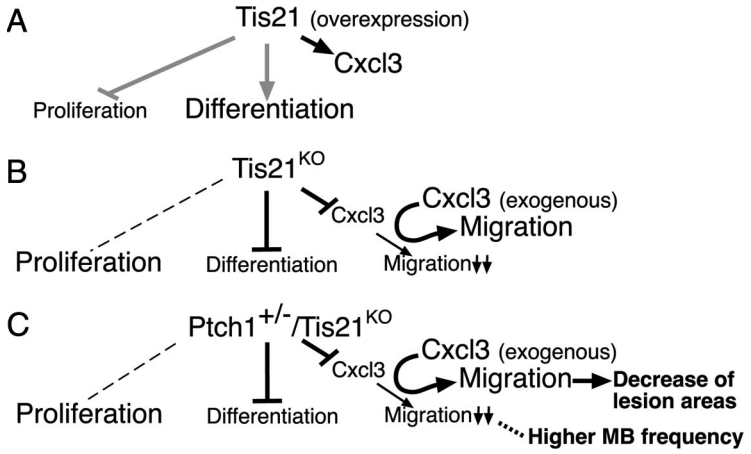

Figure 11. A working model, in conditions of gain of function of *Tis21* (***A***), or loss of function of *Tis21* in either *Ptch1*$^{+/+}$ (***B***) or *Ptch1*$^{+/-}$ context (***C***). Proliferation, differentiation, and migration out of EGL are referred to GCPs. The gray lines in ***A*** refer to data from previous reports (Canzoniere et al., 2004; Farioli-Vecchioli et al., 2007). ***B***, ***C***, In *Tis21*^{KO} and in *Ptch1*$^{+/-}$/*Tis21*^{KO} mice, the expression of *Cxcl3* in GCPs and the migration of GCPs out of EGL decrease. ***C***, In *Ptch1*$^{+/-}$/*Tis21*^{KO} mice, this decrease correlates (dotted line) with the enhancement of medulloblastoma frequency. The defect of migration is rescued in both genotypes by exogenous Cxcl3, which, in *Ptch1*$^{+/-}$/*Tis21*^{KO} mice, reduces the area of cerebellar lesions (***C***). The dashed line on the left indicates no effect on proliferation relative to controls.

trols (Fig. 10*C*,*C*′; $p = 0.020$ and $p = 0.021$, respectively). The extent of induction of the *Cxcl3* promoter by *Tis21* in PC12 cells was comparable with that exerted by TNF-α, which is a known inducer of the *Cxcl3* promoter (Anisowicz et al., 1991) ($p = 0.040$ vs control; Fig. 10*C*,*C*′).

Next, we asked whether the *Tis21*-dependent increase of *Cxcl3* promoter activity was related to recruitment of Tis21 to the *Cxcl3* promoter. We performed ChIP experiments on primary cultures of cerebellar granule neurons and on purified GCPs, obtained from P7 wild-type rats, using the anti-Tis21 antibody A3H, as described previously (Farioli-Vecchioli et al., 2009). The recruitment of Tis21 to the *Cxcl3* promoter was significantly induced in cerebellar granule neurons infected with *Tis21* virus, relative to control neurons infected with β-*Gal* virus (Fig. 10*D*; $p = 0.02$ vs column on the left). The increased association of exogenous Tis21 with the *Cxcl3* promoter sequences was specific, as it was not detected with the muscle creatine kinase promoter (negative control, inactive in cerebellar granule neurons; Fig. 10*D*; $p = 0.002$ vs column on the right). We also observed a recruitment of endogenous Tis21, although below statistical significance (Fig. 10*D*; column on the left). To further test whether endogenous Tis21 is recruited to the *Cxcl3* promoter, we analyzed GCPs isolated from rat cerebellum; the association of Tis21 with the *Cxcl3* promoter resulted significantly above the background association with the negative control promoter (threefold increase; Fig. 10*D*, graph on the right; $p = 0.02$) and was higher than that observed for endogenous Tis21 in cerebellar granule neurons. Therefore, the endogenous Tis21 protein specifically interacts with the *Cxcl3* promoter.

Together, this indicates that *Tis21* may induce the transcription of *Cxcl3* following recruitment to its promoter.

To extend and confirm our real-time PCR data indicating that *Cxcl3* is expressed like *Tis21* in purified GCPs [Fig. 8*E* and our microarray data (see Notes)], we sought to assess in cerebellum the cellular localization of Cxcl3 and Tis21 as well as that of the Cxcl3 receptor. Therefore, by *in situ* hybridization, we analyzed the expression of *Cxcl3* and *Tis21* mRNAs in the cerebellar layers of P7 *Tis21*^{WT} mice. We observed that *Tis21* and *Cxcl3* mRNAs colocalize and are very strongly expressed in GCPs within the whole EGL (Fig. 10*E*,*F*). A weaker signal appears detectable also in cerebellar granule neurons of the IGL. Moreover, Cxcr2 (i.e., the receptor of Cxcl3) (Rossi and Zlotnik, 2000) is detectable in clusters at the surface of the plasma membrane of GCPs and, to a lower extent, also in Purkinje cells and in the pial membrane (Fig. 10*G*). As Cxcl3 is a secreted chemokine, this suggests that the migration of GCPs to the ML and IGL may be controlled by Cxcl3 through an autocrine loop, regulated by *Tis21* expression.

Discussion

We have generated a new murine medulloblastoma model that enabled us to identify new mechanisms underlying the plasticity and neoplastic transformation of GCPs. In this model, the ablation of *Tis21* strikingly enhances, from 25 to 80%, the incidence of medulloblastoma spontaneously occurring in Patched1 heterozygous mice. At the origin of the higher medulloblastoma incidence is the higher frequency with which *Tis21*-null GCPs become preneoplastic in early postnatal life and cluster in the EGL, to form focal and diffused hyperplastic lesions that will develop after 12 weeks of age into medulloblastomas. In GCPs lacking *Tis21*, we observe a remarkable delay in their migration from the EGL and also from lesions, to the neighboring molecular and internal granular layers. Such an effect is intrinsic to the GCP and is peculiar to the null mutation of *Tis21*—given that *Patched1* heterozygosity by itself does not inhibit migration of GCPs. The migration defect of *Tis21*-null GCPs is quantitatively comparable with that observed in mice deprived of genes known to regulate the migration of GCPs, such as *BDNF* (Borghesani et al., 2002; Kokubo et al., 2009). Moreover, *Tis21*-null GCPs also show a delay of differentiation in the EGL but not in lesions. Surprisingly, no change is observed in the proliferation rate of GCPs lacking *Tis21*, either in the EGL or in lesions. Thus, our data indicate that *Tis21* is required for migration and terminal differentiation of GCPs, while its known action as inhibitor of proliferation of GCPs, emerging upon its upregulation (Canzoniere et al., 2004; Farioli-Vecchioli et al., 2007), appears to be redundant. In fact, it is worth noting that, in other neural and non-neural progenitor cell types, such as those of the hippocampus, subventricular zone, and muscle, or in embryo fibroblasts, the knockout of *Tis21* elicits an increase of proliferation, consistently with its physiological antiproliferative activity (Boiko et al., 2006; Evangelisti et al., 2009; Farioli-Vecchioli et al., 2009). This sug-

←

(*Figure legend continued.*) experiments with GCPs. *$p < 0.05$ versus control, Student's *t* test. ***E***, ***F***, Expression of *Tis21* and *Cxcl3* mRNAs, respectively, as detected by *in situ* hybridization in cerebellar midsagittal sections from P7 wild-type mice; their expression colocalizes and is very high in GCPs, throughout the whole EGL width. Black box, Area at higher magnification. Scale bars: 100 μm; enlargement, 20 μm. ***G***, Expression of Cxcr2, receptor of Cxcl3, immunostained by a specific antibody in a representative confocal image of a cerebellar midsagittal section from P7 wild-type mice. Nuclei are visualized by Hoechst 33258 staining. Clusters of receptors are clearly detectable in GCPs (white arrowhead in EGL) and to a lower extent in the pial membrane (PM) and in Purkinje cells (black-white arrowhead); staining of putative Bergmann's glia is indicated by white arrows. Scale bar, 25 μm.

gests that, in cerebellar progenitor cells, other genes might contribute redundantly with *Tis21* to maintain the tightly regulated control of proliferation.

It has been shown that GCPs proliferate when they are exposed to the microenvironment of the EGL proliferative niche and exit the cell cycle as a result of migrating away from this environment (Choi et al., 2005). Thus, differentiation and migration are correlated as differentiation can occur only after GCPs have migrated outside the proliferative EGL region, under control of Shh, a strong mitogen produced by Purkinje cells (Dahmane and Ruiz i Altaba, 1999; Wallace, 1999; Wechsler-Reya and Scott, 1999; Lewis et al., 2004; Choi et al., 2005). The delay in migration, detectable in *Tis21*-null GCPs, either *Patched1* wild-type or heterozygous, causes their prolonged permanence in the EGL and thus exposure to the proliferative action of Shh. We hypothesize that this may result in the higher frequency of lesions and higher incidence of medulloblastomas observed in the double-mutant genotype ($Ptch1^{+/-}/Tis21^{KO}$). It appears that, in $Ptch1^{+/-}/Tis21^{KO}$ double-mutant mice, tumorigenesis follows two steps: (1) at 2 weeks, when the EGL is still present (i.e., since the initial postnatal stages), the percentage of double-mutant mice with lesions as well as the number of lesions per cerebellum increases significantly, with respect to $Ptch1^{+/-}/Tis21^{WT}$; (2) at 12 weeks of age, the percentage of $Ptch1^{+/-}/Tis21^{WT}$ mice with lesions has decreased, while that of double-mutant mice remains high. In addition, the percentage of mice with lesions at 12 weeks of age exactly matches that of mice developing medulloblastoma. Overall, this suggests that the ablation of *Tis21* in *Patched1* heterozygous mice, by causing from the early postnatal period a lengthened exposure of GCPs in the EGL area to the transforming effect exerted by Shh, may favor their preneoplastic transformation and an additional burst of tumorigenesis after 12–15 weeks of age. This latter would result in a delayed attainment of the plateau in the medulloblastoma incidence curve, which may also explain the longer average latency of medulloblastoma onset in double mice. We cannot exclude, however, that a component of the longer latency may be a reduced diffusion of tumor GCPs and thus a reduced tumor expansion.

Our data indicated that, in *Tis21*-null mice, no change occurs in the expression of genes of known pathways regulating migration of cerebellar neurons, such as *BDNF/TrkB* (Borghesani et al., 2002; Kokubo et al., 2009), *astrotactin1/astrotactin2* (Wilson et al., 2010), and *neuregulin/Erb4* (Rio et al., 1997). However, a genome-wide expression analysis by microarray of GCPs isolated from mice at P7, followed by real-time PCR expression analysis, showed that in double-mutant mice several other genes involved in neuronal cell migration presented a highly decreased mRNA expression, namely, the chemokine *Cxcl3*, *ephrin4A* (Wilkinson, 2001), and *Jmy*, a transcriptional coactivator of p53 that regulates cell motility (Coutts et al., 2009; Zuchero et al., 2009). In particular, we noticed *Cxcl3*, as it presented a strong decrease of expression in GCPs, and even more strikingly in pGCPs of lesions in double-mutant *Patched1* heterozygous/*Tis21*-null mice, compared with *Patched1* heterozygous/*Tis21* wild-type mice. Chemokines have been described to regulate cell migration in leukocytes and in several other cell types (de Haas et al., 2007). More recently, a number of chemokines have been shown to be expressed in neurons, where they may play a role in development, synaptic transmission, and neuroinflammation (Bertollini et al., 2006; Charo and Ransohoff, 2006; Ubogu et al., 2006). Cxcl2, a chemokine closely related to Cxcl3 as it shares the same sequence of four conserved cysteines in the N-terminal region (Rossi and Zlotnik, 2000), is expressed in cerebellar granule neurons (Yabe et al., 2004). Interestingly, the genetic ablation of *CXCR4*, the receptor of the *Cxcl12* chemokine, has been shown to cause a defect of migration of cerebellar granule cells (Ma et al., 1998). Our demonstration that Cxcl3 rescues the defect of migration of GCPs of double-mutant mice, without affecting their differentiation or proliferation, points to *Cxcl3* as responsible for this defect. Indeed, the reduced migration observed in isolated GCPs silenced for *Cxcl3* expression, suggests a cell-autonomous role of *Cxcl3* in this process. Furthermore, a causal role in tumorigenesis for *Cxcl3* is strongly suggested for the first time by our observation that exogenous Cxcl3 reduces the extension of diffused lesions, which are formed by pGCPs and represent a stage contiguous to the full-blown tumor. As Cxcl3 reduces the area of lesions by inducing the migration of pGCPs outside lesions, we can speculate that this migration-promoting action of Cxcl3 may induce pGCP to exit from the neoplastic program. Moreover, we observe that the transcription of *Cxcl3* is directly controlled by *Tis21* in GCPs, where, after secretion, Cxcl3 can activate its receptor.

Together, these findings support our hypothesis of a migration defect as the cause of the enhancement of medulloblastoma tumorigenesis following *Tis21* ablation. By microarray analysis, we also identified a chemokine, *Cxcl12*, whose levels increase in the EGL of Tis21-null mutant mice. As *Cxcl12* seems to exert an action opposite to *Cxcl3*, since it promotes the localization of GCPs to the EGL by chemoattraction (Klein et al., 2001), it is also possible that the decrease of *Cxcl3* in GCPs prevents their migration outside the EGL in synergy with *Cxcl12*.

Interestingly, in line with our data, another example of a genetic defect of GCPs migration leading to increase of medulloblastoma frequency has been very recently reported, represented by *Patched1* heterozygous mice knock-out for *nitric oxide synthase* (Haag et al., 2012).

Thus, *Tis21*, by controlling chemokine levels in GCPs, can play a key role in the control of their migration (Fig. 11, model). Importantly, the expression of *Tis21* has been demonstrated to decrease in human medulloblastomas, in particular those of the desmoplastic subtype, and also in medulloblastomas of *Patched1* heterozygous mice (Farioli-Vecchioli et al., 2007). Hence, this new *Tis21/Patched1* medulloblastoma model displaying defective GCPs migration, as well as altered expression of several genes identified here, may highlight novel features of the physiopathological conditions occurring in human medulloblastoma. While it is possible that other genes identified here may concur to the defective migration of GCPs and increased lesion formation caused by ablation of *Tis21*, *Cxcl3*, being able to rescue this complex *Tis21*-dependent defective phenotype, might be investigated as a new target for medulloblastoma therapy.

Notes

Supplemental material for this article is available at http://www.inmm.cnr.it/tirone/JNsuppl.zip. The supplemental material includes supplemental Figure S1, Bergmann glia.tif, Bergmann's glia analysis in *Tis21* WT and knock-out mice, either in *Patched1* heterozygous or wild-type background; supplemental Figure S2, small.tif, which shows that RNAi knockdown of *Cxcl3* in cerebellar slices inhibits the ability of GCPs to migrate out of EGL, indicating a cell-autonomous action of *Cxcl3*; and Farioli-Vecchioli_Table S1_.xls, the original microarray data. Table S1 has not been peer reviewed.

References

Anisowicz A, Messineo M, Lee SW, Sager R (1991) An NF-κB-like transcription factor mediates IL-1/TNF-α induction of gro in human fibroblasts. J Immunol 147:520–527. Medline

Ben-Arie N, Hassan BA, Bermingham NA, Malicki DM, Armstrong D, Matzuk M, Bellen HJ, Zoghbi HY (2000) Functional conservation of atonal and Math1 in the CNS and PNS. Development 127:1039–1048. Medline

Bertollini C, Ragozzino D, Gross C, Limatola C, Eusebi F (2006) Fractalkine/CX3CL1 depresses central synaptic transmission in mouse hippocampal slices. Neuropharmacology 51:816–821. CrossRef Medline

Boiko AD, Porteous S, Razorenova OV, Krivokrysenko VI, Williams BR, Gudkov AV (2006) A systematic search for downstream mediators of tumor suppressor function of p53 reveals a major role of BTG2 in suppression of Ras-induced transformation. Genes Dev 20:236–252. CrossRef Medline

Borghesani PR, Peyrin JM, Klein R, Rubin J, Carter AR, Schwartz PM, Luster A, Corfas G, Segal RA (2002) BDNF stimulates migration of cerebellar granule cells. Development 129:1435–1442. Medline

Boukhtouche F, Janmaat S, Vodjdani G, Gautheron V, Mallet J, Dusart I, Mariani J (2006) Retinoid-related orphan receptor a controls the early steps of Purkinje cell dendritic differentiation. J Neurosci 26:1531–1538. CrossRef Medline

Cancedda L, Fiumelli H, Chen K, Poo MM (2007) Excitatory GABA action is essential for morphological maturation of cortical neurons *in vivo*. J Neurosci 27:5224–5235. CrossRef Medline

Canzoniere D, Farioli-Vecchioli S, Conti F, Ciotti MT, Tata AM, Augusti-Tocco G, Mattei E, Lakshmana MK, Krizhanovsky V, Reeves SA, Giovannoni R, Castano F, Servadio A, Ben-Arie N, Tirone F (2004) Dual control of neurogenesis by PC3 through cell cycle inhibition and induction of Math1. J Neurosci 24:3355–3369. CrossRef Medline

Charo IF, Ransohoff RM (2006) The many roles of chemokines and chemokine receptors in inflammation. N Engl J Med 354:610–621. CrossRef Medline

Choi Y, Borghesani PR, Chan JA, Segal RA (2005) Migration from a mitogenic niche promotes cell-cycle exit. J Neurosci 25:10437–10445. CrossRef Medline

Coutts AS, Weston L, La Thangue NB (2009) A transcription co-factor integrates cell adhesion and motility with the p53 response. Proc Natl Acad Sci U S A 106:19872–19877. CrossRef Medline

Dahmane N, Ruiz i Altaba A (1999) Sonic hedgehog regulates the growth and patterning of the cerebellum. Development 126:3089–3100. Medline

de Haas AH, van Weering HR, de Jong EK, Boddeke HW, Biber KP (2007) Neuronal chemokines: versatile messengers in central nervous system cell interaction. Mol Neurobiol 36:137–151. CrossRef Medline

Evangelisti C, Astolfi A, Gaboardi GC, Tazzari P, Pession A, Goto K, Martelli AM (2009) TIS21/BTG2/PC3 and cyclin D1 are key determinants of nuclear diacylglycerol kinase-zeta-dependent cell cycle arrest. Cell Signal 21:801–809. CrossRef Medline

Farioli-Vecchioli S, Tanori M, Micheli L, Mancuso M, Leonardi L, Saran A, Ciotti MT, Ferretti E, Gulino A, Pazzaglia S, Tirone F (2007) Inhibition of medulloblastoma tumorigenesis by the antiproliferative and prodifferentiative gene PC3. FASEB J 21:2215–2225. CrossRef Medline

Farioli-Vecchioli S, Saraulli D, Costanzi M, Pacioni S, Cinà I, Aceti M, Micheli L, Bacci A, Cestari V, Tirone F (2008) The timing of differentiation of adult hippocampal neurons is crucial for spatial memory. PLoS Biol 6:e246. CrossRef Medline

Farioli-Vecchioli S, Saraulli D, Costanzi M, Leonardi L, Cinà I, Micheli L, Nutini M, Longone P, Oh SP, Cestari V, Tirone F (2009) Impaired terminal differentiation of hippocampal granule neurons and defective contextual memory in PC3/Tis21 knockout mice. PLoS One 4:e8339. CrossRef Medline

Feng X, Lu X, Man X, Zhou W, Jiang LQ, Knyazev P, Lei L, Huang Q, Ullrich A, Zhang Z, Chen Z (2009) Overexpression of Csk-binding protein contributes to renal cell carcinogenesis. Oncogene 28:3320–3331. CrossRef Medline

Georgakopoulos A, Xu J, Xu C, Mauger G, Barthet G, Robakis NK (2011) Presenilin1/gamma-secretase promotes the EphB2-induced phosphorylation of ephrinB2 by regulating phosphoprotein associated with glycosphingolipid-enriched microdomains/Csk binding protein. FASEB J 25:3594–3604. CrossRef Medline

Gibson P, Tong Y, Robinson G, Thompson MC, Currle DS, Eden C, Kranenburg TA, Hogg T, Poppleton H, Martin J, Finkelstein D, Pounds S, Weiss A, Patay Z, Scoggins M, Ogg R, Pei Y, Yang ZJ, Brun S, Lee Y, et al. (2010) Subtypes of medulloblastoma have distinct developmental origins. Nature 468:1095–1099. CrossRef Medline

Goodrich LV, Milenković L, Higgins KM, Scott MP (1997) Altered neural cell fates and medulloblastoma in mouse patched mutants. Science 277:1109–1113. CrossRef Medline

Guardavaccaro D, Corrente G, Covone F, Micheli L, D'Agnano I, Starace G, Caruso M, Tirone F (2000) Arrest of G_1-S progression by the p53-inducible gene PC3 is Rb dependent and relies on the inhibition of cyclin D1 transcription. Mol Cell Biol 20:1797–1815. CrossRef Medline

Haag D, Zipper P, Westrich V, Karra D, Pfleger K, Toedt G, Blond F, Delhomme N, Hahn M, Reifenberger J, Reifenberger G, Lichter P (2012) Nos2 inactivation promotes the development of medulloblastoma in Ptch1$^{+/-}$ mice by deregulation of Gap43-dependent granule cell precursor migration. PLoS Genet 8:e1002572. CrossRef Medline

Hahn H, Wicking C, Zaphiropoulous PG, Gailani MR, Shanley S, Chidambaram A, Vorechovsky I, Holmberg E, Unden AB, Gillies S, Negus K, Smyth I, Pressman C, Leffell DJ, Gerrard B, Goldstein AM, Dean M, Toftgard R, Chenevix-Trench G, Wainwright B, et al. (1996) Mutations of the human homolog of *Drosophila* patched in the nevoid basal cell carcinoma syndrome. Cell 85:841–851. CrossRef Medline

Hahn H, Wojnowski L, Zimmer AM, Hall J, Miller G, Zimmer A (1998) Rhabdomyosarcomas and radiation hypersensitivity in a mouse model of Gorlin syndrome. Nat Med 4:619–622. CrossRef Medline

Hatten ME (1999) Central nervous system neuronal migration. Annu Rev Neurosci 22:511–539. CrossRef Medline

Hatten ME, Roussel MF (2011) Development and cancer of the cerebellum. Trends Neurosci 34:134–142. CrossRef Medline

Heard E, Rougeulle C, Arnaud D, Avner P, Allis CD, Spector DL (2001) Methylation of histone H3 at Lys-9 is an early mark on the X chromosome during X inactivation. Cell 107:727–738. CrossRef Medline

Kadin ME, Rubinstein LJ, Nelson JS (1970) Neonatal cerebellar medulloblastoma originating from the fetal external granular layer. J Neuropathol Exp Neurol 29:583–600. CrossRef Medline

Kessler JD, Hasegawa H, Brun SN, Emmenegger BA, Yang ZJ, Dutton JW, Wang F, Wechsler-Reya RJ (2009) N-myc alters the fate of preneoplastic cells in a mouse model of medulloblastoma. Genes Dev 23:157–170. CrossRef Medline

Kim JY, Nelson AL, Algon SA, Graves O, Sturla LM, Goumnerova LC, Rowitch DH, Segal RA, Pomeroy SL (2003) Medulloblastoma tumorigenesis diverges from cerebellar granule cell differentiation in patched heterozygous mice. Dev Biol 263:50–66. CrossRef Medline

Klein RS, Rubin JB, Gibson HD, DeHaan EN, Alvarez-Hernandez X, Segal RA, Luster AD (2001) SDF-1 alpha induces chemotaxis and enhances Sonic hedgehog-induced proliferation of cerebellar granule cells. Development 128:1971–1981. Medline

Kokubo M, Nishio M, Ribar TJ, Anderson KA, West AE, Means AR (2009) BDNF-mediated cerebellar granule cell development is impaired in mice null for CaMKK2 or CaMKIV. J Neurosci 29:8901–8913. CrossRef Medline

Lee Y, Miller HL, Jensen P, Hernan R, Connelly M, Wetmore C, Zindy F, Roussel MF, Curran T, Gilbertson RJ, McKinnon PJ (2003) A molecular fingerprint for medulloblastoma. Cancer Res 63:5428–5437. Medline

Lewis PM, Gritli-Linde A, Smeyne R, Kottmann A, McMahon AP (2004) Sonic hedgehog signaling is required for expansion of granule neuron precursors and patterning of the mouse cerebellum. Dev Biol 270:393–410. CrossRef Medline

Livak KJ, Schmittgen TD (2001) Analysis of relative gene expression data using real-time quantitative PCR and the $2^{-\Delta\Delta C(T)}$ method. Methods 25:402–408. CrossRef Medline

Lu Q, Sun EE, Klein RS, Flanagan JG (2001) Ephrin-B reverse signaling is mediated by a novel PDZ-RGS protein and selectively inhibits G protein-coupled chemoattraction. Cell 105:69–79. CrossRef Medline

Lumpkin EA, Collisson T, Parab P, Omer-Abdalla A, Haeberle H, Chen P, Doetzlhofer A, White P, Groves A, Segil N, Johnson JE (2003) Math1-driven GFP expression in the developing nervous system of transgenic mice. Gene Expr Patterns 3:389–395. CrossRef Medline

Ma Q, Jones D, Borghesani PR, Segal RA, Nagasawa T, Kishimoto T, Bronson RT, Springer TA (1998) Impaired B-lymphopoiesis, myelopoiesis, and derailed cerebellar neuron migration in CXCR4- and SDF-1-deficient mice. Proc Natl Acad Sci U S A 95:9448–9453. CrossRef Medline

Marino S (2005) Medulloblastoma: developmental mechanisms out of control. Trends Mol Med 11:17–22. CrossRef Medline

Miyata T, Maeda T, Lee JE (1999) NeuroD is required for differentiation of the granule cells in the cerebellum and hippocampus. Genes Dev 13:1647–1652. CrossRef Medline

Oliver TG, Read TA, Kessler JD, Mehmeti A, Wells JF, Huynh TT, Lin SM, Wechsler-Reya RJ (2005) Loss of patched and disruption of granule cell development in a pre-neoplastic stage of medulloblastoma. Development 132:2425–2439. CrossRef Medline

O'Neill LP, Turner BM (1995) Histone H4 acetylation distinguishes coding regions of the human genome from heterochromatin in a differentiation-dependent but transcription-independent manner. EMBO J 14:3946–3957. Medline

Park S, Lee YJ, Lee HJ, Seki T, Hong KH, Park J, Beppu H, Lim IK, Yoon JW, Li E, Kim SJ, Oh SP (2004) B-cell translocation gene 2 (Btg2) regulates vertebral patterning by modulating bone morphogenetic protein/smad signaling. Mol Cell Biol 24:10256–10262. CrossRef Medline

Passeri D, Marcucci A, Rizzo G, Billi M, Panigada M, Leonardi L, Tirone F, Grignani F (2006) Btg2 enhances retinoic acid-induced differentiation by modulating histone H4 methylation and acetylation. Mol Cell Biol 26:5023–5032. CrossRef Medline

Pietsch T, Waha A, Koch A, Kraus J, Albrecht S, Tonn J, Sörensen N, Berthold F, Henk B, Schmandt N, Wolf HK, von Deimling A, Wainwright B, Chenevix-Trench G, Wiestler OD, Wicking C (1997) Medulloblastomas of the desmoplastic variant carry mutations of the human homologue of *Drosophila* patched. Cancer Res 57:2085–2088. Medline

Polleux F, Giger RJ, Ginty DD, Kolodkin AL, Ghosh A (1998) Patterning of cortical efferent projections by semaphorine-neuropilin. Science 282:1904–1906. CrossRef Medline

Pomeroy SL, Tamayo P, Gaasenbeek M, Sturla LM, Angelo M, McLaughlin ME, Kim JY, Goumnerova LC, Black PM, Lau C, Allen JC, Zagzag D, Olson JM, Curran T, Wetmore C, Biegel JA, Poggio T, Mukherjee S, Rifkin R, Califano A, et al. (2002) Prediction of central nervous system embryonal tumour outcome based on gene expression. Nature 415:436–442. CrossRef Medline

Qiu Z, Cang Y, Goff SP (2010) Abl family tyrosine kinases are essential for basement membrane integrity and cortical lamination in the cerebellum. J Neurosci 30:14430–14439. CrossRef Medline

Raffel C, Jenkins RB, Frederick L, Hebrink D, Alderete B, Fults DW, James CD (1997) Sporadic medulloblastomas contain PTCH mutations. Cancer Res 57:842–845. Medline

Rio C, Rieff HI, Qi P, Khurana TS, Corfas G (1997) Neuregulin and erbB receptors play a critical role in neuronal migration. Neuron 19:39–50. CrossRef Medline

Rossi D, Zlotnik A (2000) The biology of chemokines and their receptors. Annu Rev Immunol 18:217–242. CrossRef Medline

Schüller U, Heine VM, Mao J, Kho AT, Dillon AK, Han YG, Huillard E, Sun T, Ligon AH, Qian Y, Ma Q, Alvarez-Buylla A, McMahon AP, Rowitch DH, Ligon KL (2008) Acquisition of granule neuron precursor identity is a critical determinant of progenitor cell competence to form Shh-induced medulloblastoma. Cancer Cell 14:123–134. CrossRef Medline

Stoppini L, Buchs PA, Muller D (1991) A simple method for organotypic cultures of nervous tissue. J Neurosci Methods 37:173–182. CrossRef Medline

Thomas WD, Chen J, Gao YR, Cheung B, Koach J, Sekyere E, Norris MD, Haber M, Ellis T, Wainwright B, Marshall GM (2009) Patched1 deletion increases N-Myc protein stability as a mechanism of medulloblastoma initiation and progression. Oncogene 28:1605–1615. CrossRef Medline

Ubogu EE, Cossoy MB, Ransohoff RM (2006) The expression and function of chemokines involved in CNS inflammation. Trends Pharmacol Sci 27:48–55. CrossRef Medline

Wallace VA (1999) Purkinje-cell-derived Sonic hedgehog regulates granule neuron precursor cell proliferation in the developing mouse cerebellum. Curr Biol 9:445–448. CrossRef Medline

Wang VY, Zoghbi HY (2001) Genetic regulation of cerebellar development. Nat Rev Neurosci 2:484–491. CrossRef Medline

Wechsler-Reya RJ, Scott MP (1999) Control of neuronal precursor proliferation in the cerebellum by Sonic hedgehog. Neuron 22:103–114. CrossRef Medline

Weyer A, Schilling K (2003) Developmental and cell type-specific expression of the neuronal marker NeuN in the murine cerebellum. J Neurosci Res 73:400–409. CrossRef Medline

Wilkinson DG (2001) Multiple roles of EPH receptors and ephrins in neural development. Nat Rev Neurosci 2:155–164. CrossRef Medline

Wilson PM, Fryer RH, Fang Y, Hatten ME (2010) Astn2, a novel member of the astrotactin gene family, regulates the trafficking of ASTN1 during glial-guided neuronal migration. J Neurosci 30:8529–8540. CrossRef Medline

Wolter M, Reifenberger J, Sommer C, Ruzicka T, Reifenberger G (1997) Mutations in the human homologue of the *Drosophila* segment polarity gene patched (PTCH) in sporadic basal cell carcinomas of the skin and primitive neuroectodermal tumors of the central nervous system. Cancer Res 57:2581–2585. Medline

Yabe T, Herbert JT, Takanohashi A, Schwartz JP (2004) Treatment of cerebellar granule cell neurons with the neurotrophic factor pigment epithelium-derived factor in vitro enhances expression of other neurotrophic factors as well as cytokines and chemokines. J Neurosci Res 77:642–652. CrossRef Medline

Yang ZJ, Ellis T, Markant SL, Read TA, Kessler JD, Bourboulas M, Schüller U, Machold R, Fishell G, Rowitch DH, Wainwright BJ, Wechsler-Reya RJ (2008) Medulloblastoma can be initiated by deletion of Patched in lineage-restricted progenitors or stem cells. Cancer Cell 14:135–145. CrossRef Medline

Zhokhov SS, Desfeux A, Aubert N, Falluel-Morel A, Fournier A, Laudenbach V, Vaudry H, Gonzalez BJ (2008) Bax siRNA promotes survival of cultured and allografted granule cell precursors through blockade of caspase-3 cleavage. Cell Death Differ 15:1042–1053. CrossRef Medline

Zuchero JB, Coutts AS, Quinlan ME, Thangue NB, Mullins RD (2009) p53-cofactor JMY is a multifunctional actin nucleation factor. Nat Cell Biol 11:451–459. CrossRef Medline